International Journal of Coal Geology 173 (2017) 110–128

Contents lists available at ScienceDirect

International Journal of Coal Geology

journal homepage: www.elsevier.com/locate/ijcoalgeo

The Miocene coal seams in the Soma Basin (W. Turkey): Insights from coal petrography, mineralogy and geochemistry

Ali İhsan Karayiğit [a,*], Ralf Littke [b], Xavier Querol [c], Tim Jones [d], R. Görkem Oskay [a,1], Kimon Christanis [e]

[a] Hacettepe University, Department of Geological Engineering, 06800 Ankara, Turkey
[b] Institute of Geology and Geochemistry of Petroleum and Coal, Energy and Mineral Resources (EMR), RWTH Aachen University, Lochnerstr. 4-20, 52056 Aachen, Germany
[c] Institute of Environmental Assessment and Water Research (IDÆA), Consejo Superior de Investigaciones Científicas (CSIC), C/JordiGirona 18-26, 08034 Barcelona, Spain
[d] Department of Earth Sciences, Cardiff University, Cardiff CF1 3YE, UK
[e] University of Patras, Department of Geology, Rio, Patras, Greece

ARTICLE INFO

Article history:
Received 27 January 2017
Received in revised form 4 March 2017
Accepted 5 March 2017
Available online 6 March 2017

Keywords:
Coal
Tuff
Element
Rock-Eval pyrolysis
Coal facies
Miocene
Soma
Turkey

ABSTRACT

The Neogene Soma Basin, western Turkey, hosts three coal seams (kM2, kM3 and kP1) and several altered tuff layers within the Miocene sequences. This study focuses on the evaluation of coal-petrography, mineralogical and elemental compositions, as well as the Rock-Eval pyrolysis of the three coal seams from Eynez, Işıklar and Deniş sectors, and to identify the mineralogy of altered tuff layers within kM2 and kP1 seams. The routine coal quality analyses show that coal samples from the kM2 seam are characterized by lower ash yields and total S contents, and higher gross calorific values than kM3 and kP1 seams. The mineralogical composition of the bulk coal samples varies between all three seams. The statistical treatment implies that major elements in bulk coal samples such as Al, Fe, K, Mg and Na, and the vast majority of minor and trace elements have inorganic affinity. The trace element contents and elemental enrichments in the coal samples are generally changeable from seam to seam, which could be related to differences in ash yield and mineralogy. Altered tuff layers, or tonsteins were identified in kM2 and kP1 seams. The tonsteins are clay rich, and certain trace elements (e.g. As and Zr) are enriched in the coal layers beneath the tuff layers in the kM2 seam. This might be related to penetration of leached pore water into these layers and precipitation of epigenetic minerals.

The coal-petrography composition and the coal-facies diagrams show that the precursor peat of the kM2 seam was accumulating under telmatic, mesotrophic, anoxic conditions, whereas the water level was high and stable. The relatively low ash yields and thicker coal beds suggest a lower clastic input from the basin margins, and water table fluctuations resulted in calcareous intercalations in the kM3 and kP1 seams. These imply the development of limno-telmatic conditions whereas fluvial activity affected during peat accumulation of both seams. Considering the maceral composition along with the coal thickness, coal seams in the Soma Basin might display oil-generation potential; however, the pyrolysis analysis shows that the studied coal seams are mainly gas-prone and only certain coal beds have mixed-hydrocarbon generation capacity. All data presented in this study indicates that lithological features, differences in coal qualities and elemental contents in the Soma Basin were mainly controlled by changes in the depositional conditions and the detrital input during Miocene.

1. Introduction

The regional extensional tectonic regime during late Cenozoic resulted in the development of regional volcanic activity and the formation of several NW–SE and NE–SW trending grabens in the western Turkey (Seyitoğlu and Scott, 1991; Yılmaz et al., 2000). Terrestrial conditions were also predominant during Neogene. The grabens were filled in with alluvial, fluvial and lacustrine sediments, and volcanosedimentary rocks. Suitable climatic conditions along with constant subsidence allowed peat accumulation within these basins during Miocene; therefore, several economic coal deposits are located within Miocene lacustrine and terrestrial sequences in the western Turkey (Toprak, 2009; Kayseri-Özer, 2017).

The Soma Basin hosts the most significant coal deposits in the western Turkey. The total coal reserves of the Soma Basin are about 738 Mt; about 10.4 Mt coal are annually produced by mainly open-pit mines, of which annually 7.7 Mt are consumed in Soma coal-fired power plants with 990 MW total installed capacity, whereas 2.7 Mt are used for domestic heating and industrial purposes (TKİ-ELİ, 2015). The basin is divided into several sectors, and hosts three coal seams, kM2 (lower-seam), kM3 (middle-seam) and kP1 (upper-seam). The coal features and the thickness of these seams vary from sector to sector (Tuncalı

* Corresponding author.
E-mail address: aik@hacettepe.edu.tr (A.İ. Karayiğit).
[1] Visiting scholar.

http://dx.doi.org/10.1016/j.coal.2017.03.004
0166-5162/

et al., 2002). Another distinct feature of the Soma Basin is the presence of several altered tuff layers and basaltic intrusions within the coal seams (Karayiğit and Whateley, 1997). The tuff layers, particularly identified within the kM2 seam, could be useful for stratigraphic correlation during underground mining operations and can also give information about mineral input during peat accumulation.

Several studies dealing with Soma Basin mainly focused on geological setting, palynological, environmental and economic aspects (Nebert, 1978; Akgün et al., 1986; Gemici et al., 1991; Takahashi and Jux, 1991; Akgün, 1993; İnci, 1998a,b, 2002; Karayiğit et al., 2000, 2006; Vassilev et al., 2005; Tercan et al., 2013; Hokerek and Ozcelik, 2015; Baysal et al., 2016; Kayseri-Özer, 2017). Petrographical and geochemical studies of coals in this area are limited (Karayiğit and Whateley, 1997; Karayiğit, 1998; Tuncalı et al., 2002; Bulut and Karayiğit, 2006; Toprak, 2009). All these studies focused on either certain mining sectors or the suitability of coal for power plants, and none of them reported any correlation among the coal seams within the basin. It is noteworthy that detailed study on altered tuff layers within the coal seams is also lacking. In this paper, the main goal is to determine coal features, to reconstruct the palaeoenvironmental conditions during peat accumulation, and to determine the oil-and gas-generation potential of the kM2, kM3 and kP1 coal seams at the Eynez, Işıklar and Deniş sectors, using coal petrography, mineralogy and geochemical techniques. The specific aim of the study is to identify the features of tuff layers occurring within the seams and to assess their impacts on mineralogical and elemental compositions of the coal seams.

2. Geological setting

The Soma Basin is a NE–SW trending, approximately 20-km long and 5-km wide, fault-controlled basin in western Turkey (Seyitoğlu and Scott, 1991; İnci, 2002). The margins of the basin are mainly built of Upper Cretaceous-Palaeocene carbonates (recrystallized limestone) and Miocene volcanic rocks; furthermore, small greywacke and diabase blocks are outcrop on southern margin (Fig. 1a). The regional extensional tectonics initiated during the early Miocene, created depositional space for the basinal infillings (Nebert, 1978; Seyitoğlu and Scott, 1996; İnci, 1998a); consequently, the major coal-bearing Soma Formation started deposition during Early to Middle Miocene (Benda, 1971; İnci, 2002). The Formation is composed of alluvial sediments and lacustrine carbonates which host the kM2 and kM3 seams (Fig. 1b). The total thickness of the kM2 seam reaches up to 27 m, whereas the kM3 seam with thicker calcareous intercalations reaches up to 15 m. The overlaying Deniş Formation (Fig. 1b) commenced with alluvial sedimentation and turned to fluvial sediments and lacustrine carbonates along with the kP1 seam (İnci, 2002). The total thickness of the kP1 seam is variable within the basin; it is only mineable at the Deniş sector. This seam hosts several coal layers and thick intercalations (fossiliferous claystone and clayey limestone/marl); therefore, it can be distinguished into lower, middle and upper parts. The Pliocene Soma volcanics overlie the Deniş Formation (Fig. 1b). Furthermore, Pliocene-Pleistocene basaltic intrusions caused the contact metamorphism in the kM2 coal seam resulting in natural coke occurrences near to the contact zone (Karayiğit and Whateley, 1997; Karayiğit, 1998). Finally, Quaternary unconsolidated sediments unconformably overlay the older units (Fig. 1b).

3. Material and methods

A total of 64 coal samples and 18 intercalations samples, of which 6 samples are from altered tuff layers, 7 samples from clayey limestone/marl, 4 samples from claystone and 1 sample from fine grained sandstone, were gathered using channel sampling technique from five profiles in the Eynez, Işıklar and Deniş sectors (Fig. 2). The kM2 seam was

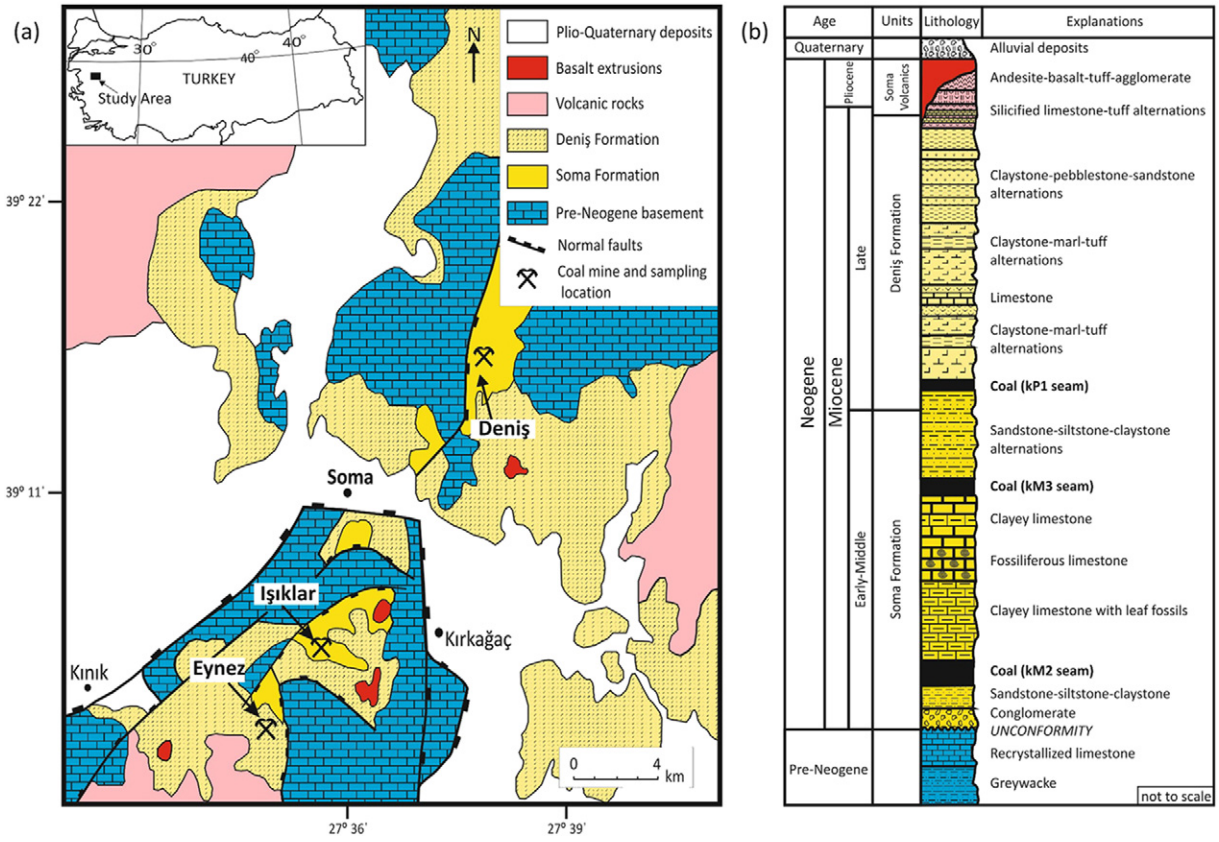

Fig. 1. a) Geological map of surrounding area of the Soma Basin (modified from İnci (1998a), Karayiğit (1998)); (b) Stratigraphic column of the Soma Basin (modified and simplified from Karayiğit and Whateley (1997), İnci (1998a)).

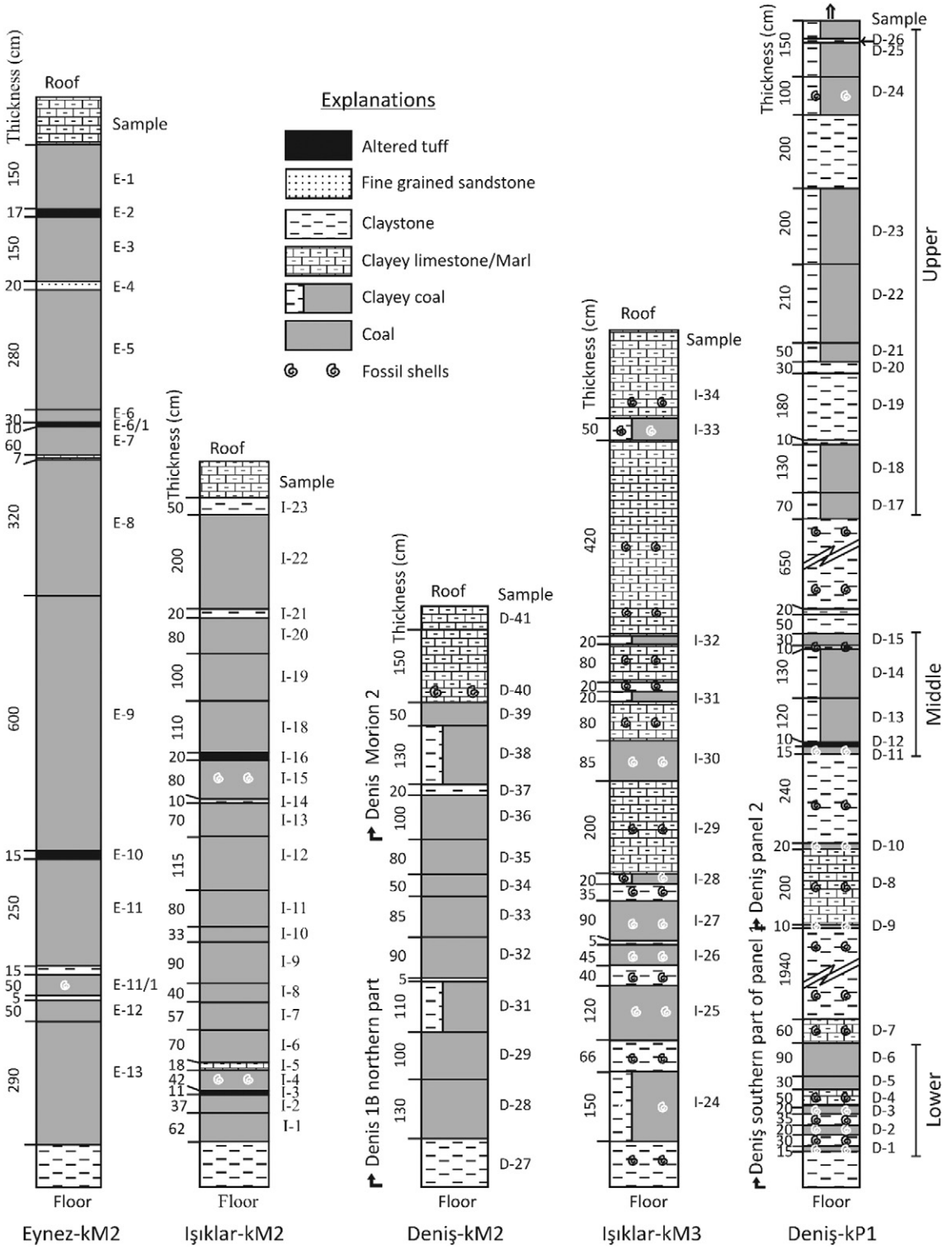

Fig. 2. Stratigraphic column of the studied profiles in the Soma Basin.

sampled from Eynez, Işıklar and Deniş sectors, whereas kM3 was only sampled at the Işıklar sector and kP1 at the Deniş sector.

Standard proximate and ultimate analyses were conducted according to ASTM standards (ASTM D3175, 2011; D3174, 2012; D3302, 2015; D5373, 2016). The gross calorific values were determined in an IKA 4000 adiabatic calorimeter (ASTM D5865, 2013) at Hacettepe University. The instruments calibrated with certificated standard materials for coal of the LECO Co. The petrographic analysis was performed on polished coal blocks, prepared according to ISO 7404-2 (2009). The blocks were examined in oil immersion under both white incident light and blue-light excitation using a Zeiss Axioplan coal at RWTH Aachen University and a Leica DM4000M microscope at Hacettepe University. The maceral identification followed the ICCP System 1994 (ICCP, 1994, 2001; Sýkorová et al., 2005; Pickel et al., 2017). Random huminite reflectance was measured on ulminite B according to ISO 7404-5 (2009). The Tissue Preservation Index (TPI), the Vegetation Index (VI),

the Groundwater Influence (GWI) and the Gelification Index (GI) (Calder et al., 1991; Diessel, 1992) were based on the formulas of Kalkreuth et al. (1991) and modified by Kalaitzidis et al. (2004) for low-rank Cenozoic coals. These calculations were based on maceral composition. The mineralogical composition of bulk coal and inorganic samples was determined using an X-ray diffractometer with a Cu anode tube at Hacettepe University and Cardiff University. The clay fraction analysis (XRD-CF) was also carried out on selected inorganic samples at Hacettepe University according to methodology explained by Poppe et al. (2001). The selected samples were prepared using oriented aggregate mounts technique and the XRD analyses are performed from the mounts after the glycol and heat treatments (550 °C). The XRD results were checked with the XRD patterns of raw samples.

The Rock-Eval pyrolysis was conducted to determine the T_{max}, Hydrogen Index (HI) and the Oxygen Index (OI) values according to the procedure described by Espitalié et al. (1977a,b). Total organic carbon (TOC) and inorganic carbon (TIC) contents were determined using a LECO RC-412 Multiphase C/H/H_2O Analyzer at RWTH Aachen University. Combustion took place in oxygen current at temperatures between 350 °C and 520 °C for TOC and 520 °C and 1050 °C for TIC. Moreover, a brief organic-geochemical analysis was only performed on two bulk coal samples, namely one from the kM2 seam (E-9) and another from the kP1 seam (D-6), using Soxhlet extraction with dichloromethane and GC–MS. The GC–MS analyses were performed using a Finnigan MAT 95 mass spectrometer linked to a Hewlett Packard Series II 5890 gas chromatograph, which was equipped with a 30 mxx 0.25 mm i.d. × 0.25 μm film thickness ZB-1 fused silica column. The identification of compounds was based on correlation of mass spectra and gas chromatographic retention with selected published data (e.g., Peters and Moldowan, 1993; Weiss et al., 2000). For more detailed information about this technique can be found in Bechtel et al. (2016) and Ghazwani et al. (2016).

The elemental composition was determined by means of inductively coupled plasma atomic emission spectrometry (ICP-AES) and inductively coupled plasma mass spectrometry (ICP-MS) at the Institute of Environmental Assessment and Water Research (IDAEA) applying the technique described in detail by Querol et al. (1995). The results are also checked using an international SARM 19 standard. Polished blocks of selected coal and tuff samples were carbon coated and examined under SEM equipment situated at Hacettepe University, Cardiff University and RWTH Aachen University in order to have an insight in the mineralogical composition and the trace elements contained in the minerals.

4. Results

4.1. Macroscopic features and proximate analysis of coal

The matrix lithotype is commonly identified in kM2 coal, whereas the mineral-rich lithotype is more abundant in the kM3 seam, particularly in the middle and upper parts of the kP1 seam. Gastropod shell-bearing coal beds were more common in the kM3 seam and the lower parts of the kP1 seam, whereas the clay bands within coal beds were abundant in the upper section of the kP1 seam (Fig. 2). The floor is mainly composed of claystone and the roof of clayey limestone/marl. The kM2 seam hosts thin intercalations being mainly composed of claystone/clayey limestone (Fig. 2). The kM3 seam hosts mainly calcareous intercalations, whereas gastropod-bearing claystone is more abundant in the kP1 seam. Furthermore, altered tuff layers were mainly identified in the kM2 seam at Eynez and Işıklar sectors (Fig. 2); one tuff layer was also identified in the kP1 seam at the Deniş sector.

The results of proximate analysis along with the gross calorific values indicate that there are several significant differences between the coal seams in the Soma Basin (Table 1). The ash yields in the kM2 seam are generally lower than in other seams. Ash yields exceeding 50% (on dry basis) are mostly related to frequent existence of gastropod remains within coal beds in kM3 and kP1 seams. In turn, high volatile matter yields (up to 67.6%, on dry, ash-free basis) and low calorific values are recorded (Table 1). The proximate analysis results and the calorific values are generally in agreement with previous studies; higher ash yields are only reported from kP1 in this study (Karayiğit et al., 2000; Tuncalı et al., 2002; Tercan et al., 2013). This may be related to differences of sampling intervals and/or location of sampling profile at the Deniş sector.

4.2. Maceral composition and rank

Huminite, liptinite and inertinite macerals vary in proportions in all three seams (Table 2). Huminite is the dominant maceral group (up to 84.9 vol%, on whole coal basis) and its proportions are slightly higher in the upper parts of the kM2 seam and lowest parts of the kP1 seam The kM2 seam is characterized by high telohuminite content with the highest value recorded at the Deniş sector (61.2 vol%), whereas the kM3 and kP1 seams contain higher detrohuminite contents (Table 2). Ulminite, mainly eu-ulminite, is predominant within the telohuminite subgroup (Fig. 3a); however, texto-ulminite dominates in samples of the kM2 seam from Işıklar and Deniş sectors (Fig. 3d). Furthermore,

Table 1
Ranges and weighted averages (in parenthesis) of the values obtained from proximate and ultimate analyses, and Rock-Eval pyrolysis of the coal samples from the Soma Basin (CV: calorific value, TOC: total organic carbon, TIC: total inorganic carbon, HI: hydrogen index, OI: oxygen index, PI: production index; BI: bitumen index, QI: quality index, ar: as received; adb: air-dry basis; db: dry basis; daf: dry, ash-free basis; maf: moist, ash-free basis).

Seam/Sector	kM2			kM3	kP1
	Eynez	Işıklar	Deniş	Işıklar	Deniş
Total moisture (wt%, ar)	11.1–17.8 (14.7)	7.5–16.8 (11.8)	13.7–20.7 (18.3)	9.6–14.5 (11.2)	14.4–25.6 (18.7)
Ash (wt%, db)	3.7–32.3 (16.2)	4.1–37.3 (12.1)	4.2–42.2 (249.6)	14.5–56.9 (36.2)	7.6–64.7 (45.3)
Volatile matter (wt%, daf)	42.9–58.7 (54.8)	42.6–55.6 (46.2)	46.4–59.4 (52.1)	46.7–62.2 (56.8)	47.1–67.6 (57.6)
Gross CV (MJ/kg, maf)	22.7–26.5 (24.8)	20.9–27.7 (25.2)	16.2–23.2 (20.6)	18.0–25.0 (21.5)	13.2–21.5 (17.1)
Total S (wt%, db)	0.4–2.1 (0.8)	0.2–2.0 (1.0)	0.2–1.6 (0.6)	2.4–3.5 (3.1)	0.5–5.0 (1.7)
TC (%, adb)	45.5–64.5 (56.2)	39.3–64.5 (57.3)	34.5–57.6 (43.5)	23.8–55.4 (38.7)	18.5–57.0 (31.7)
TOC (%, adb)	45.4–64.4 (56.0)	38.5–64.3 (56.7)	32.5–57.4 (42.7)	23.4–54.8 (38.0)	17.9–56.9 (31.1)
TIC (%, adb)	0.1–0.5 (0.3)	0.1–2.4 (0.6)	0.2–2.0 (0.7)	0.1–2.1 (0.7)	0.1–4.7 (0.6)
S1 (mg HC/g rock)	1.1–2.4 (1.5)	1.0–3.7 (1.7)	1.2–3.3 (2.3)	0.6–1.2 (0.9)	0.7–1.9 (1.0)
S2 (mg HC/g rock)	62.8–107.2 (83.5)	56.7–103.2 (77.7)	33.7–83.1 (51.7)	35.5–55.5 (43.6)	22.2–71.9 (36.6)
S3 (mg HC/g rock)	7.0–12.1 (10.7)	9.8–15.1 (12.8)	4.5–16.9 (8.6)	7.9–15.1 (10.4)	3.2–19.4 (5.6)
T_{max} (°C)	413–427 (420)	410–426 (418)	392–420 (411)	420–439 (431)	412–430 (424)
HI (mg HC/g TOC)	121–173 (149)	109–178 (137)	88–145 (121)	92–152 (120)	76–142 (120)
OI (mg HC/g rock)	15–20 (19)	21–25 (23)	13–37 (20)	25–34 (28)	14–41 (18)
PI (S1 / (S1 + S2))	0.01–0.03 (0.02)	0.01–0.04 (0.02)	0.03–0.05 (0.04)	0.01–0.03 (0.02)	0.02–0.03 (0.03)
BI (S1 / TOC)	0.02–0.04 (0.03)	0.02–0.06 (0.03)	0.03–0.07 (0.05)	0.01–0.05 (0.03)	0.02–0.05 (0.04)
QI ((S1 + S2) / TOC)	1.2–1.8 (1.5)	1.1–1.8 (1.4)	0.9–1.5 (1.2)	0.9–1.5 (1.2)	0.8–1.4 (1.2)

Table 2
Coal-petrography results of the coal samples from the Soma Basin (TH: telohuminite, DH: detrohuminite, GH: gelohuminite, H: huminite. I: inertinite, L: liptinite, MM: mineral matter, $\%R_o$: random reflectance, SD: standard deviation).

Seam	Sector	Sample	TH	DH	GH	H	L	I	MM	$\%R_o \pm SD$
			(vol% on whole basis)							
kM2	Eynez	E-1	44.4	32.1	8.4	84.9	6.3	1.1	7.7	0.46 ± 0.02
		E-3	37.2	30.6	4.7	72.5	5.5	0.6	21.4	0.46 ± 0.02
		E-5	36.9	28.5	5.5	70.9	6.8	0.2	22.1	0.45 ± 0.02
		E-6	23.0	25.2	3.5	51.7	9.9	0.6	37.8	0.44 ± 0.02
		E-7	48.3	30.8	5.5	84.6	11.4	0.6	3.4	0.44 ± 0.01
		E-8	31.2	17.8	4.1	53.1	7.5	0.8	38.6	0.46 ± 0.02
		E-9	36.3	14.1	2.0	52.4	7.7	2.3	37.6	0.45 ± 0.02
		E-11	35.3	18.8	4.3	58.4	12.3	1.0	28.3	0.44 ± 0.01
		E-11/1	29.7	13.0	3.5	46.2	9.0	0.4	44.4	0.45 ± 0.02
		E-12	35.0	10.0	2.4	47.4	10.3	1.0	41.3	0.45 ± 0.02
		E-13	35.3	15.9	3.1	54.3	8.8	3.3	33.6	0.45 ± 0.03
	Işıklar	I-22	42.3	28.1	10.0	80.4	9.0	0.4	10.2	0.44 ± 0.01
		I-20	49.0	16.9	12.6	78.5	7.4	3.2	10.9	0.44 ± 0.01
		I-19	52.6	17.7	13.3	83.6	7.7	0.4	8.3	0.44 ± 0.01
		I-18	42.2	13.3	6.5	62.0	6.4	0.2	31.4	0.43 ± 0.01
		I-15	46.2	19.6	7.6	73.4	12.4	–	14.2	0.44 ± 0.02
		I-13	37.4	23.2	7.2	67.8	14.0	0.2	18.0	0.42 ± 0.02
		I-12	47.1	13.2	7.4	67.7	9.5	0.6	22.2	0.44 ± 0.01
		I-11	44.6	16.1	5.6	66.3	9.9	0.4	23.4	0.43 ± 0.01
		I-10	18.5	12.5	2.4	33.4	5.4	–	61.2	0.44 ± 0.01
		I-9	55.3	7.8	5.7	68.8	9.0	0.2	22.0	0.44 ± 0.02
		I-8	41.0	12.0	4.5	57.5	10.0	0.6	31.9	0.42 ± 0.01
		I-7	39.3	6.8	4.7	50.8	3.9	0.4	44.9	0.43 ± 0.01
		I-6	33.7	15.2	2.5	51.4	9.8	2.9	35.9	0.43 ± 0.01
		I-4	25.6	12.2	3.3	41.1	7.7	0.4	50.8	0.42 ± 0.01
		I-2	24.4	8.9	3.3	36.6	5.7	0.2	57.5	0.42 ± 0.01
		I-1	41.6	16.2	6.0	63.8	16.9	0.8	18.5	0.43 ± 0.02
	Deniş	D-39	61.2	6.7	9.5	77.4	7.1	–	15.5	0.37 ± 0.02
		D-38	20.9	13.1	2.4	36.4	11.3	0.6	51.7	0.39 ± 0.02
		D-36	25.9	7.5	4.3	37.7	4.8	0.4	57.1	0.39 ± 0.01
		D-35	37.9	17.3	4.7	59.9	9.0	0.2	30.9	0.36 ± 0.02
		D-34	23.8	6.7	3.0	33.5	4.0	–	62.5	0.37 ± 0.02
		D-33	41.9	9.0	6.3	57.2	11.2	–	31.6	0.37 ± 0.01
		D-32	42.7	14.5	7.2	64.4	7.8	0.4	27.4	0.38 ± 0.02
		D-31	39.4	10.7	4.6	54.7	14.3	0.2	30.8	0.38 ± 0.01
		D-29	22.0	18.1	6.4	46.5	6.2	0.2	47.1	0.39 ± 0.02
		D-28	30.0	17.7	5.7	53.4	9.5	–	37.1	0.40 ± 0.02
kM3	Işıklar	I-33	20.0	30.9	10.6	61.5	9.5	10.2	18.8	0.46 ± 0.02
		I-32	7.4	15.3	4.4	27.1	6.9	11.0	55.0	0.45 ± 0.03
		I-31	23.9	37.8	9.7	71.4	7.4	8.9	12.3	0.46 ± 0.02
		I-30	6.7	30.3	2.6	39.6	8.2	5.7	46.5	0.46 ± 0.03
		I-28	20.4	39.0	7.3	66.7	6.1	4.1	23.1	0.45 ± 0.02
		I-27	5.5	32.7	3.3	41.5	6.1	4.9	47.5	0.45 ± 0.03
		I-26	9.4	26.9	3.4	39.7	4.2	5.8	50.3	0.46 ± 0.02
		I-25	4.8	27.6	1.9	34.3	6.5	3.3	55.9	0.46 ± 0.02
		I-24	5.7	7.5	2.3	15.5	5.2	1.2	78.1	0.45 ± 0.02

ulminite macerals are well gelified in Eynez and Işıklar coal (both kM2 and kM3 seams, Fig. 3d, g, and h). Textinite contents are low (≤1 vol%) in the samples. The cell-lumens of textinite are generally filled in with corpohuminite, resinite and/or mineral matter (Fig. 3b). Densinite is predominant within the detrohuminite group. Inertodetrinite, liptodetrinite and sporinite are mostly associated with densinite (Fig. 3c, e, and h). Gelohuminite is also commonly observed in all studied samples (Table 2). Corpohuminite is the dominant maceral in this subgroup (up to 11.5 vol%). Gelinite, however, is more common gelohuminite maceral in lower and middle parts of the kP1 seam. Liptinite is also commonly observed in all samples (1.7 and 16.9 vol%) and liptodetrinite is the predominant liptinite maceral. In addition, liptinite contents are slightly high in the kM2 seam, where resinite is also commonly identified. Inertinite contents are generally low in the kM2 seam (≤1 vol%), whereas these are slightly higher than others (up to 11.0 vol%) in the kM3 seam and increased upwards in the seam. Minerals identified under coal-petrography microscopy are mainly clay minerals, carbonates (calcite and siderite) and pyrite (Fig. 3f). Gastropod-shell fragments are also commonly observed. The maceral composition of the studied samples is generally in agreement with the previous coal-petrography studies from the Soma Basin (Karayiğit and Whateley, 1997; Karayiğit, 1998; Tuncalı et al., 2002; Bulut and Karayiğit, 2006; Toprak, 2009), but also some circum-Mediterranean Cenozoic coals (Querol et al., 1996 and refs. therein).

The random huminite reflectance ($\%R_o$) measured on eu-ulminite B, varies between 0.36 and 0.46%. The higher R_o values were measured on coal samples from the kM2 seam at the Eynez sector and the kM3 seam at the Işıklar sector; low R_o values were measured from the kM2 seam at the Deniş sector (Table 2). Considering the presence of basalt dykes in the adjacent Eynez and Işıklar sectors (Karayiğit, 1998), deeper burial depths and presence of well-gelified ulminite in these sectors, the low R_o values from the kM2 seam in the Deniş sector can be expected. The reflectance data are in agreement with previous studies (Karayiğit and Whateley, 1997; Tuncalı et al., 2002; Toprak, 2009). The mean random reflectance along with the calorific values and the ash yields of the kM2 and kM3 indicate medium- to high-grade, low rank A to medium rank D coal and subbituminous coal (low-rank A) according to E.C.E-U.N. (1998) and ISO 11760 (2005) classifications, respectively. The kP1 coal is low- to medium-grade, low rank C to B and lignite (low-rank B) to subbituminous (low-rank A).

4.3. Bulk geochemical parameters

The kM2 coal is characterized by high total C (34.5–64.5%; on dry basis) and low total S contents (0.2–2.1%; on dry basis), while the kM3 and kP1 samples display higher total S (up to 5.0%; on dry basis) and lower total C (up to 57.0%, on dry basis) contents (Table 1). The Rock Eval analysis reveals that S1, S2 and S3 values range from 0.6 to 3.7 mg HC/g, 22.2 to 107.2 mg HC/g, 3.2 to 19.4 mg HC/g coal, respectively. The kM2 seam coal reveals the highest mean S1 and S2 values (Table 1). Total organic carbon (TOC) values of the kM2 seam range from 32.5 to 64.4 wt% (on air-dried basis) and their mean values are relatively higher than these of other seams. In the kM3 and kP1 seams TOC values vary from 23.4 to 54.8 wt% (avg. 38.0 wt%) and 17.9 to 56.9 wt% (avg. 31.1 wt%). Total inorganic carbon (TIC) contents are relatively high in fossil shell-bearing samples (Table 1). Moreover, TOC values are higher in the upper parts of the kM2 and kM3 seams where ash yields are lower. The total sulphur contents of the seams in the Soma Formation display a slight increase upwards; in addition to this, higher total sulphur contents are generally recorded above and beneath altered tuff layers in the kM2 seam. In contrast, while ash yields increase upwards in the kP1 seam, TOC values, total carbon and sulphur contents decrease.

The Hydrogen Index (HI) values are generally low and range from 76 to 178 mg HC/g TOC (Fig. 4 and Table 1), and their calculated HI_{max} values on the HI-VR diagram are between 241 and 278 mg HC/g TOC (Fig. 5). The Oxygen Index (OI) is generally low (≤41 mg CO_2/g TOC; Fig. 4a and Table 1). T_{max} values vary between 392° and 439 °C being characteristic for a low-rank coal. The HI vs. OI and HI vs. T_{max} diagrams (Fig. 4) show that kerogen type III is dominant in all seams, and in some samples mixed types III and IV are common (Tissot and Welte, 1984). Furthermore, plotting data on HI vs. T_{max} diagram indicates that the kM2 and kM3 coal samples are immature to early mature and samples from the kP1 seam are clearly immature (Espitalié et al., 1977a,b). Overall, the results of Rock-Eval analysis indicate that the coal samples have heterogeneity in organic matter that is characteristic for low-rank coals (Petersen et al., 2009; Escobar et al., 2016). This heterogeneity is also in agreement with the results of the coal-petrography examination. For instance, changes in HI values seem to be related to variable maceral contents (Hunt, 1991; Petersen and Rosenberg, 2000; Kalaitzidis et al., 2009; Petersen et al., 2009; Gross et al., 2015). The kM2 seam displays higher telohuminite and HI values, whereas relatively low HI and high OI and S3 values can be testimony for relatively high inertinite contents of the kM3 seam. The high total S contents generally tend to elevate HI values (Petersen, 2006); in contrast, the effect of total S on HI values in the studied samples might be limited due to low coal rank.

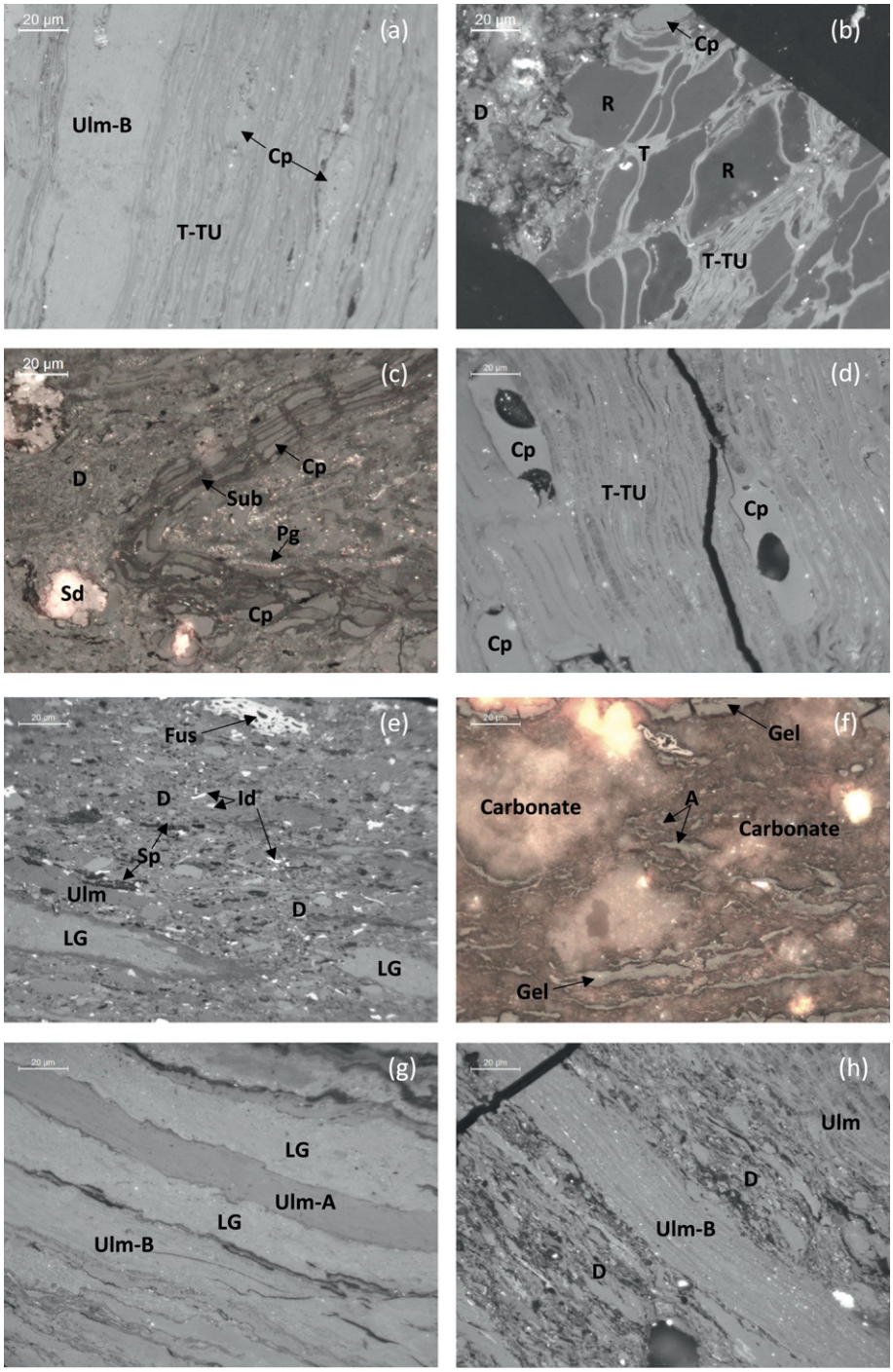

Fig. 3. Photomicrographs of Soma coal are taken on polished blocks under incident white light (a, c, e, f, g, h), oil immersion, 500x total magnification. Textinite (T), texto-ulminite (TU), ulminite (Ulm), ulminite-A (Ulm-A), ulminite-B (Ulm-B), densinite (D), attrinite (A), corpohuminite (Cp), gelinite (Gel), levigelinite (LG), porigelinite (Pg), fusinite (Fus), inertodetrinite (Id) resinite (R), sporinite (Sp), suberinite (Sub), and siderite (Sd).

4.4. Molecular organic geochemistry

Preliminary organic-geochemical analysis on only two samples provides us with basic understanding about the predominant peat-forming vegetation in the kM2 and kP1 seams. Most abundant substances in the aliphatic fraction of the analysed coal samples can be attributed to cyclic sesquiterpenes and cyclic diterpenes. The E-9 sample (kM2 seam) was dominated by these substances (Fig. 6a). Beside cyclic sesquiterpenes and cyclic diterpenes, *n*-alkenes are also present with their chain lengths between 10 and 31 carbon atoms. In both samples (E-9 and D-6) a bimodal distribution with maxima at C_{14}/C_{15} and around C_{23}/C_{25} are observed (Fig. 6b and d). Sample D-6 (kP1 seam) exhibits the highest concentrations of *n*-alkenes at $C_{23}/C_{25}/C_{27}/C_{29}$ (Fig. 6d), but the *n*-alkenes of sample E-9 maximised at C_{14}/C_{15} (Fig. 6b). The maxima in the range of C_{23} and C_{25} (Fig. 6c and d) point to a high contribution of freshwater aquatic macrophytes (Ficken et al., 2000; Bechtel et al., 2016), whereas *n*-alkenes with chain lengths of >29 carbon atoms can be attributed to the input of organic matter derived from higher land plants (Volkman, 1986; Canuel et al., 1997). These distributions are in agreement with coal petrography data. The

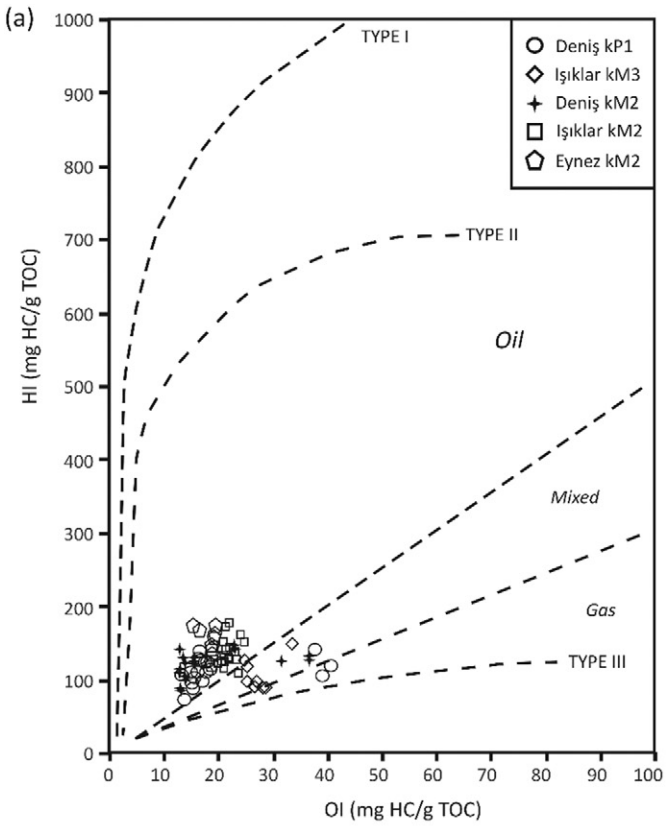

Fig. 4. The Soma coal samples projected on (a) the pseudo-Van Krevelen diagram, (b) plot of HI against T_{max} of the coal samples (after Peters (1986)).

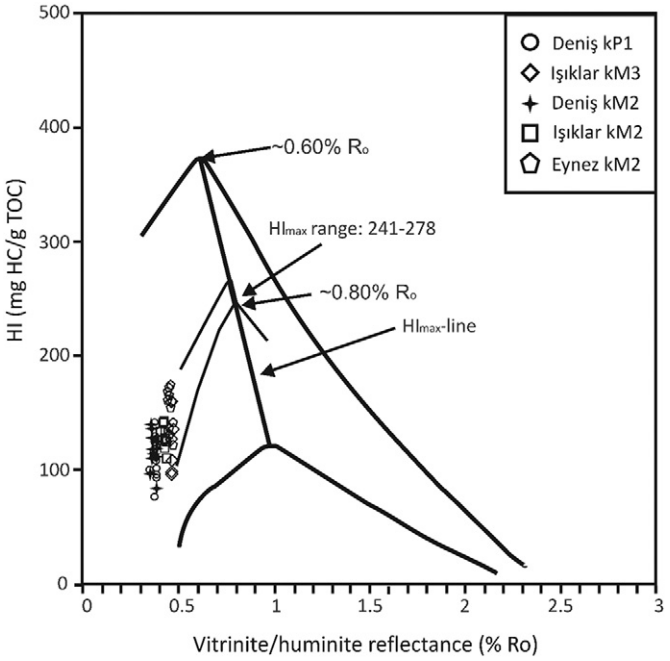

Fig. 5. The Soma coals plotted on the HI-VR diagram (after Petersen (2006)).

telohuminite group is predominant in the E-9 and D-6 samples displays higher detrohuminite contents. Furthermore, the *n*-alkene distributions of both samples are characterized significantly by an odd-over-even predominance indicating immature conditions (Fig. 6b and d).

4.5. Mineralogical composition

4.5.1. Minerals in intercalations and altered tuff layers

The common carbonate minerals in the intercalations are calcite, dolomite and siderite being dominant phases in the clayey limestone/marl (Table 3). Moreover, aragonite is only identified in gastropod shell-bearing samples. The clay minerals are the dominant phase in claystone and a minor phase in the calcareous intercalations. The results of XRD-CF analyses indicate that kaolinite and smectite are common in clay-fraction minerals in the kM2 seam, whereas in the kP1 seam illite along with kaolinite is more common. Quartz and feldspar are abundant to minor phases in the claystone; nevertheless, quartz is the dominant phase in the fined grained sandstone of the kM2 seam. Opal/CT is traced only in claystone of kM2 and kP1 seams, which also include altered tuff layers. Pyrite is also traced in a few samples from kM2 and kP1 seams (Table 3). The predominance of silicate minerals in the intercalations implies fluvial influx from marginal areas. In contrast, the Ca-rich water originated from karstic aquifers along with the lacustrine conditions allowed carbonate precipitation, particularly in the kM3 seam and the lower parts of the kP1 seam. Similar explanations were also provided by İnci (1998a).

The mineralogical composition of tuff layers in the kM2 and kP1 seams are slightly different than other intercalations. The clay minerals are the dominant phase in all layers according to the XRD results, and the abundant phases are quartz and feldspars (Table 3). Furthermore, carbonate minerals (calcite and dolomite) and opal/CT are traced in some altered tuff samples. The SEM-EDX data show a variety of accessory minerals in these layers (Table 4 and Fig. 7) such as biotite with Ti traces, phosphate (Cl-apatite and crandallite), zircon, Ti-oxides, ilmenite, titanite, REE-bearing silicates (e.g. allanite), and sulphides (pyrite, sphalerite and chalcopyrite). Beside sulphide and carbonate minerals, all these accessory minerals are identified as typical minerals for tonsteins (Bohor and Triplehorn, 1993; Ruppert and Moore, 1993; Burger et al., 2000; Dai et al., 2011, 2014; Spears, 2012), as well as

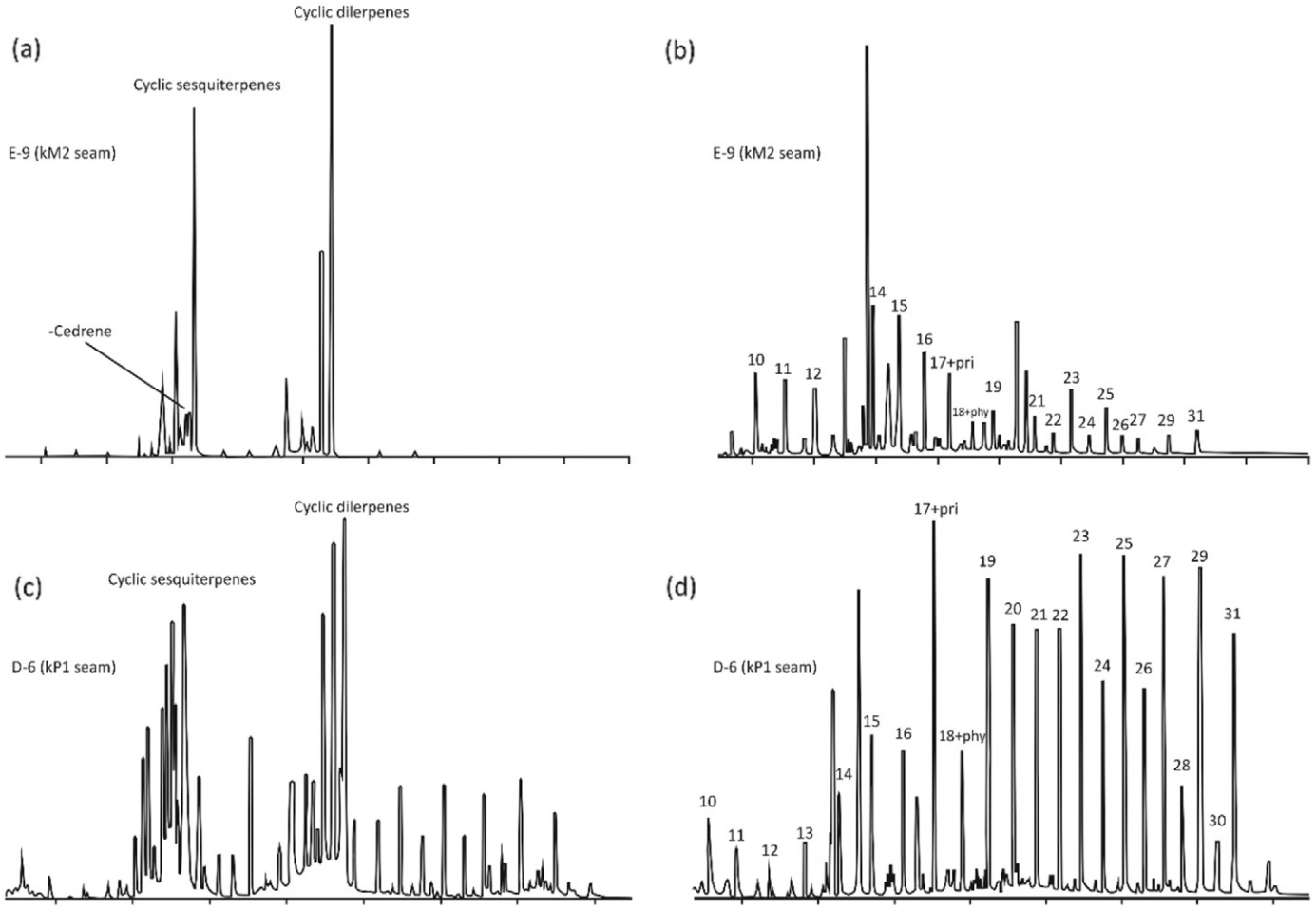

Fig. 6. Gas chromatograms of the aromatic hydrocarbon fractions of (a) cyclic compounds and (b) alkanes in sample E-9 from kM2 seam, and (c) cyclic compounds and (d) alkanes in sample D-6 from kP1 seam (*n*-alkanes are indicated by their carbon chain length, pri: pristane, phy: phytane).

Table 3
Composition of the altered volcanic ashes, inorganic sediments and coal samples from the Soma Basin based on XRD and SEM (+++ = dominant phase, ++ = abundant phase, + = minor phase, ± = detected in a few samples by XRD, a: accessory mineral detected by SEM-EDX).

Mineral	Altered tuff			Inorganic sediments					Coal				
	kM2		kP1	kM2			kM3	kP1	kM2			kM3	kP1
	Eynez	Işıklar	Deniş	Eynez	Işıklar	Deniş	Işıklar	Deniş	Eynez	Işıklar	Deniş	Işıklar	Deniş
Quartz	++	+	++	+++	++	+++		+	+++	+++	+++	+	++
Opal/CT	±		+		±			±	±		±	±	±
Clay minerals	+++	+++	+++	++	+++	++	+	++	+++	++	++	++	+++
Feldspar	+		++	+	+	±		±	±	±	±	±	±
Biotite	a	a	a						a	a			a
Titanite			a										a
Allanite			a										
Zircon	a	a	a						a	a	a		
Pyrite	a	a	+					±	+	+	±	++	+
Sphalerite		a	a						a		a		a
Chalcopyrite		a							a		a		a
Gypsum												±	±
Barite	a	a	a						a	a	a	a	a
Calcite	+			+	±	+	+++	+++	++	+++	++	+++	++
Aragonite						±	++					+	±
Dolomite	±		+	+	±	±		±	±		±		±
Ankerite										a			
Siderite					±	±		±	±	±	±		±
Apatite	a	a	a						a	a	a	a	a
Crandallite	a	a	a										
Monazite													a
Chromite										a			
Ti-oxides		a	a							a		a	a

Table 4
Summarized ranges and weighted averages of the elements (in μg/g, except otherwise cited) from the Soma Basin and their comparison with worldwide coals.

Elements	kM2						kM3		kP1		Most world coals[a]	Clarke value (for low-rank coals)[b]
	Eynez		Işıklar		Deniş		Işıklar		Deniş			
	Range	Avg.	Range	Avg.	Range	Avg.	Range	Avg.	Range	Avg.		
Al, %	0.13–3.91	1.93	0.03–5.5	1.3	0.31–6.0	3.8	0.09–8.4	3.9	0.24–9.3	6.2	–	–
Ca,%	0.26–1.78	1.02	0.40–9.2	1.1	0.69–6.4	1.9	0.36–10.1	4.4	0.92–13.4	1.5	–	–
Fe, %	0.03–1.01	0.51	0.08–2.4	0.5	0.24–1.2	0.68	0.09–1.9	1.18	0.17–2.2	1.4	–	–
K, %	<0.02–0.24	0.10	0.00–0.46	0.1	0.02–0.58	0.26	0.01–0.43	0.24	0.02–0.91	0.52	–	–
Mg, %	0.03–0.20	0.10	0.04–0.71	0.1	0.05–0.33	0.24	0.02–0.28	0.22	0.03–0.60	0.39	–	–
Na, %	<0.01–0.28	0.06	0.00–0.05	0.03	0.03–0.16	0.08	0.002–0.06	0.04	0.01–0.16	0.08	–	–
Li	1.3–39	19	0.53–89	19	2.5–96	51	1.6–339	137	1.35–232	139	1–80	10
Be	0.12–1.0	0.49	0.02–1.1	0.47	0.36–2.2	1.3	0.01–3.5	1.5	0.09–3.8	2.7	0.1–15	1.2
B	27–465	141	8.8–484	215	300–1813	578	36–578	372	213–956	503	5–400	56
P	22–271	158	15–1143	157	28–666	217	23–524	377	24–2074	443	10–3000	200
Sc	<0.01–7.2	2.9	<0.90–5.9	1.6	1.8–8.1	5.6	0.18–11	6.3	1.7–17	9.6	1–10	4.1
Ti	41–1671	643	7.4–1450	444	120–2176	1374	47–4009	1849	98–3501	2432	10–2000	720
V	12.3–228	93	5.7–206	74	33–221	157	9.7–296	155	37–369	266	2–100	22
Cr	2.1–35	21	0.57–51	15	9.8–60	41	2.1–84	44	4.7–99	68	0.5–60	15
Mn	7.4–130	52	6.9–320	56	9.9–228	64	2.0–50	32	6.4–173	57	5–300	100
Co	0.13–5.9	2.7	0.15–7.6	2.3	1.7–6.2	4.7	0.28–9.5	4.4	1.0–17	8.4	0.5–30	4.2
Ni	<2.4–20	7.3	0.63–25	9.8	13–31	23	<0.30–37	13	5.6–74	41	0.5–50	9.0
Cu	1.5–25	14	0.47–22	10	4.8–35	22	0.80–49	23	4.6–43	32	0.5–50	15
Zn	16–85	32	4.7–119	58	43–515	140	1.9–121	55	15.6–273	169	5–300	18
Ga	0.4–8.5	4.3	0.08–11	3.0	1.41–13	8.4	0.22–18	8.0	0.61–21	14	1–20	5.5
Ge	<0.10–1.3	0.54	0.03–1.2	0.5	0.28–1.2	0.85	0.03–2.5	1.1	0.66–4.2	1.8	1–50	2.0
As	8.8–66	37	6.0–242	70	1.8–15	6.5	0.55–25	18	3.2–22	7.6	0.5–80	7.6
Rb	0.23–41	9.5	0.21–63	9.0	1.7–54	27	0.33–34	14	0.70–70	40	2–50	10
Sr	15–140	54	3.4–223	40	18–250	99	13.1–271	189	13–523	108	15–500	120
Y	0.73–11	6.6	0.20–13.7	4.7	3.6–23	15	0.40–34	14	0.40–33	23	2–50	8.6
Zr	2.6–58	22	0.55–50	19	20–79	56	1.7–190	75	12.4–214	147	5–200	35
Nb	0.46–9.8	3.2	0.06–5.5	2.2	2.8–11.5	7.6	0.24–15	7.0	1.1–17	12	3–30	11
Mo	0.29–2.0	0.94	0.002–1.5	0.54	0.07–1.1	0.63	0.27–3.3	1.5	0.37–4.5	1.3	0.1–10	2.2
Cd	0.02–0.79	0.40	0.03–2.3	0.43	0.03–7.6	2.4	0.07–2.8	1.3	0.09–5.5	2.3	0.1–3	0.24
Sn	<0.14–1.4	0.41	<0.02–1.3	0.2	0.03–1.5	1.0	<0.01–2.3	0.9	0.01–2.6	1.7	1–10	0.79
Sb	0.14–0.94	0.28	<0.10–0.17	0.02	<0.02–0.44	0.15	0.02–0.4	0.3	<0.10–0.92	0.5	0.5–10	0.84
Cs	0.09–13.5	6.0	0.13–20	4.6	0.56–7.9	4.7	0.20–23	8.9	0.61–23	7.3	0.1–5	0.98
Ba	34–207	130	12–635	133	113–347	247	29–993	511	112–659	248	20–1000	150
La	1.1–15	8.4	0.1–16	5.2	3.2–25	16	0.41–49	21	0.85–48	32	1–40	10
Ce	2.1–25	13	0.21–24	8.45	5.9–44	28	0.61–80	35	1.7–77	51	2–70	22
Pr	0.25–3.0	1.7	0.03–3.1	1.1	0.73–5.2	3.3	0.09–10	4.4	0.22–9.7	6.5	1–10	3.5
Nd	0.92–12	6.8	0.12–12	4.3	3.0–21	13	0.37–40	18	0.85–39	26.2	3–30	11
Sm	0.14–1.8	1.0	0.02–2.0	0.65	0.47–3.2	2.1	0.05–5.8	2.5	0.13–5.8	3.8	1–6	1.9
Eu	0.03–0.47	0.25	0.01–0.50	0.17	0.13–0.76	0.5	0.01–1.4	0.65	0.04–1.4	0.92	0.1–2	0.5
Gd	0.16–2.1	1.2	0.03–2.4	0.83	0.64–4.1	2.7	0.06–6.6	2.9	0.12–6.8	4.6	0–4	2.6
Tb	0.02–0.30	0.16	0.003–0.35	0.11	0.09–0.56	0.37	0.01–0.88	0.38	0.02–0.90	0.61	0.1–1	0.32
Dy	0.10–1.8	0.95	0.02–2.1	0.68	0.53–3.3	2.2	0.06–5.0	2.2	0.08–5.2	3.5	1–4	2.0
Ho	0.02–0.34	0.18	0.004–0.40	0.13	0.10–0.64	0.4	0.01–0.94	0.41	0.01–0.96	0.7	0.1–2	0.5
Er	0.06–0.95	0.49	0.01–1.1	0.36	0.25–1.8	1.1	0.03–2.5	1.1	0.03–2.6	1.8	1–3	0.85
Tm	0.01–0.17	0.08	0.002–0.20	0.06	0.05–0.31	0.20	0.01–0.43	0.19	0.01–0.45	0.31	0.5–3	0.31
Yb	0.06–1.1	0.52	0.01–1.2	0.39	0.27–1.9	1.2	0.03–2.7	1.2	0.04–2.7	1.9	0.3–3	1.0
Lu	0.01–0.17	0.09	0.002–0.21	0.07	0.05–0.32	0.20	0.01–0.45	0.20	0.01–0.46	0.3	0.03–1	0.19
Hf	0.09–1.7	0.64	0.01–1.5	0.5	0.28–2.2	1.4	0.05–5.1	2.1	0.11–5.1	3.6	0.4–5	1.2
Ta	0.05–0.68	0.23	0.003–0.51	0.2	0.14–1.0	0.6	0.03–1.3	0.6	0.02–1.6	1.0	0.1–2	0.26
W	0.07–2.0	0.59	<0.10–6.8	0.74	<0.34–2.9	1.5	0.21–2.3	1.1	<0.15–4.2	1.7	0.5–5	1.2
Tl	0.01–1.31	0.25	0.001–1.6	0.27	0.10–0.65	0.35	0.01–1.3	0.6	0.06–2.8	1.1	0.2–1	0.68
Pb	1.4–25.2	11	0.36–12	5.9	6.3–41	21	0.31–53	23	1.1–73	39	2–80	6.6
Bi	0.05–0.26	0.17	<0.01–0.16	0.03	<0.12–0.46	0.3	0.01–0.72	0.3	0.01–0.86	0.5	2–20	0.84
Th	0.47–6.4	2.5	0.04–5.8	1.8	0.73–11	6.3	0.13–23	9.3	0.37–20	13	0.5–10	3.3
U	3.8–35	16	0.52–25	14	3.5–25	14	2.0–20.2	16	2.6–48	27	0.5–10	2.9

[a] From Swaine, 1990.
[b] From Ketris and Yudovich, 2009.

altered tuffs in coal-bearing sequences as reported by Kramer et al. (2001), Creech (2002), Grevenitz et al. (2003), and Zhao et al. (2016a). In this context, minerals such as quartz, biotite, feldspars, opal/CT, Cl-apatite and zircon, are primary probably products of volcanic input. Zircon crystals are generally sharp edges and/or euhedral crystals (Fig. 7a) being characteristic for volcanic origin and also for short distance transportation (Zhou et al., 1994; Burger et al., 2002; Spears, 2012; Arbuzov et al., 2016). Feldspar in the altered tuff layers could also provide indications about the volcanic activity around the basin during the Miocene (Fig. 7b and d). The SEM-EDX data shows that plagioclase is more commonly determined in the analysed tuff samples from kM2 seam, and alkali feldspars in the sample from kP1 seam. This difference is presumably related to changes in chemistry of volcanic rocks during Miocene around the Soma Basin (Ersoy et al., 2012).

The kaolinite is observed in the altered tuff layers as individual bodies (vermicules? Fig. 7e and f), associated with biotite (Fig. 7b), or around feldspar (Fig. 7c) or composed of the matrix of mineral aggregates (Figs. 7a). The latter one contains traces of mostly Ti, and lesser Fe and K; the existence of these trace elements reveals that kaolinite is mainly an alteration by-product of biotite and feldspars. Such alterations are expected considering the freshwater palaeoenvironment in

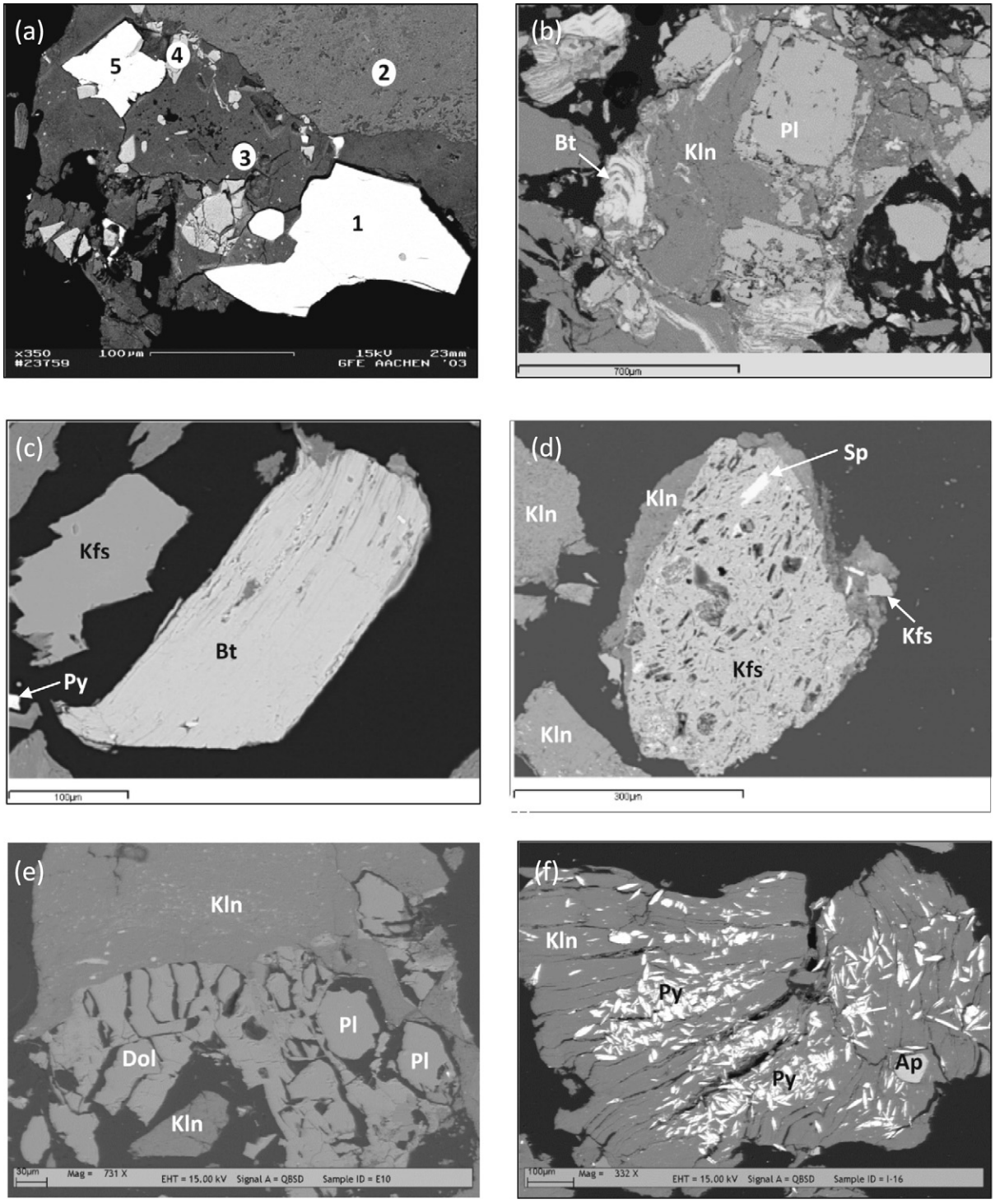

Fig. 7. SEM backscattered images of crystalline phases in the altered volcanic ash samples. a) K-feldspar (2), zircon (1 and 5) and apatite (4) associated with kaolinite (3); b) kaolinite (Kln) around possibly altered biotite (Bt) and plagioclase (Pl); c) non-altered biotite (Bt), K-feldspar (Kfs) and pyrite (Py); d) Sphalerite (Sp) within the altered K-feldspar (Kfs), and individual kaolinites (Kln) and around altered K-feldspar; e) plagioclase (Pl) and secondary dolomite (Dol) around kaolinite (Kln); d) apatite (Ap), alkali feldspar (Afs) and plagioclase (Pl) associated with kaolinite (Kln); f) pyrite (Py) blades and apatite (Ap) within kaolinite (Kln).

the Soma Basin. The presence of Ti may also indicate substitution of Ti for Al in the developing kaolinite crystals in the acidic conditions (Ward et al., 1999; Shoval et al., 2008; Dai et al., 2015a). Furthermore, the presence of pyrite blades (Fig. 7f) and the lack of zeolite minerals also imply that the alteration of tuff layers took place in the open system under slightly acidic conditions (Querol et al., 1997; Bechtel et al., 2014). Nevertheless, rare carbonate minerals (e.g. dolomite) indicating neutral conditions, are also contained (Fig. 7c). Other sulphide minerals like sphalerite and chalcopyrite seem to be developed from leached water during diagenetic stages (Arbuzov et al., 2016). The acidic conditions might also allow the reaction between weathered glass and P deriving from organic matter (Triplehorn et al., 1991) resulting in formation of alumina-phosphate minerals. Furthermore, allanite can easily alter in the depositional environment (Bohor and Triplehorn, 1993); however, its presence in the kP1 tuff layer suggests that the alteration of the tuff layers was presumably not dense as seen in the kM2 seam. Overall,

the mineralogical composition of altered tuff layers denotes that these may originate from intermediate and/or felsic volcanic rocks. Therefore, these tuff layers in kM2 and kP1 seams were derived from synchronous volcanic activity in the basin's neighbourhood.

4.5.2. Minerals in coal

The dominant phases contained in the kM2 coal are quartz and clay minerals, whereas calcite is also dominant in certain coal samples from Işıklar and Deniş sectors (Table 3). Other carbonate minerals identified in the kM2 coal are dolomite and siderite. Nevertheless, carbonate minerals are dominant in the kM3 coal, where fossil shell remains are commonly observed, and here aragonite is also identified. The upper part of the kP1 seam is characterized by the predominance of clay minerals, while calcite along with quartz is common in the lower part. Feldspars and pyrite are generally minor phases in the three seams (Table 3). Additionally, opal/CT and gypsum are also traced in few samples. The results of SEM examination are in agreement with the XRD data and provide a variety of accessory minerals (Figs. 8 and 9), such as ankerite, apatite, barite, biotite, chalcopyrite, chromite, monazite, sphalerite, titanite, Ti-oxides and zircon. Furthermore, calcareous fossil shell-fragments are also common (Fig. 8e) and fossil bone remains of Ca-phosphate composition in few samples too.

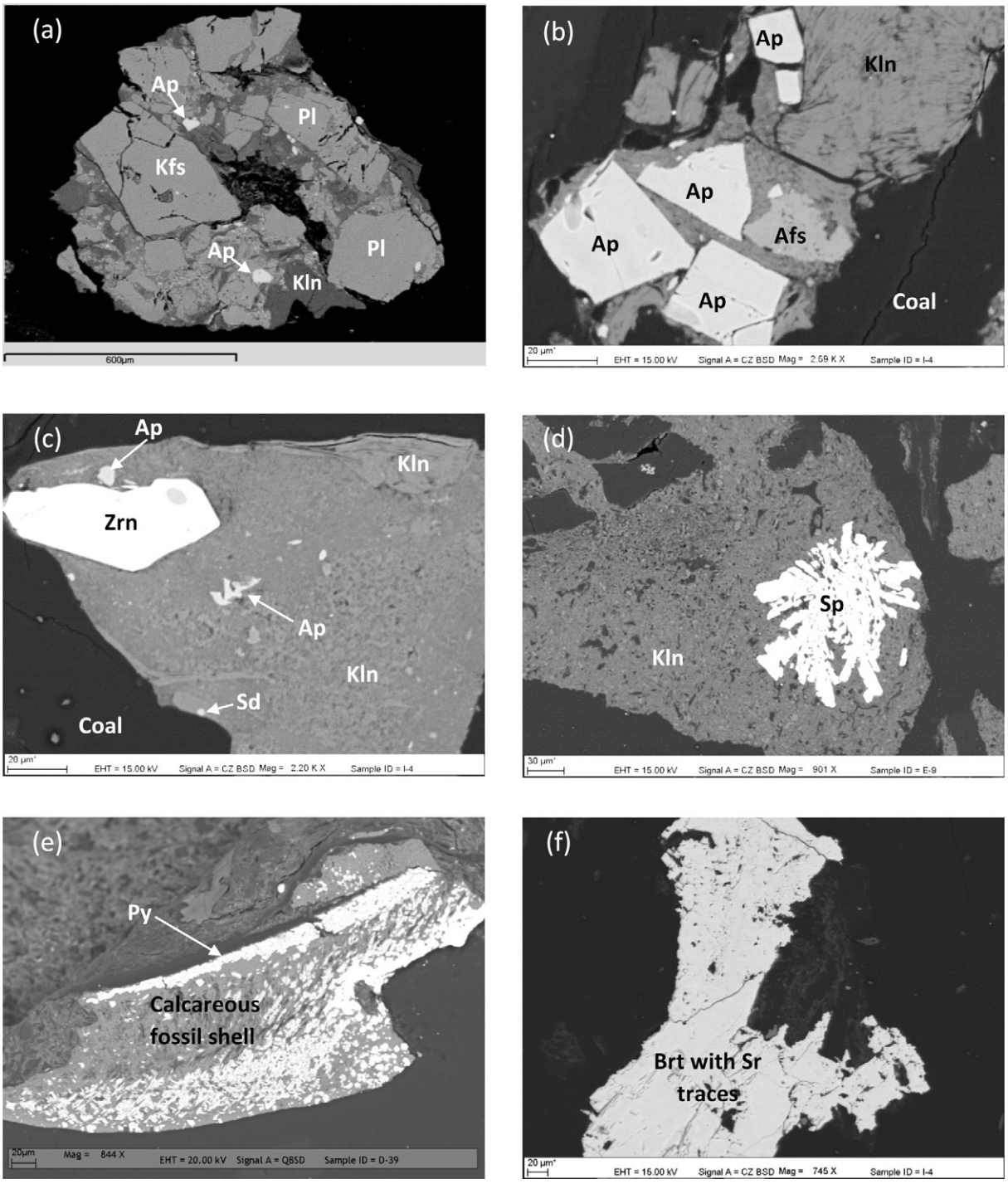

Fig. 8. SEM backscattered images of crystalline phases in the coal samples. a, b and c) apatite (Ap), siderite (Sd), zircon (Zrn) plagioclase (Pl) K-feldspar (Kfs) and alkali feldspar (Afs) associated with kaolinite (Kln); d) epigenetic sphalerite (Sp) within kaolinite (Kln); e) pyrites (Py) within the cavities of calcareous fossil shell remain; f) epigenetic barite.

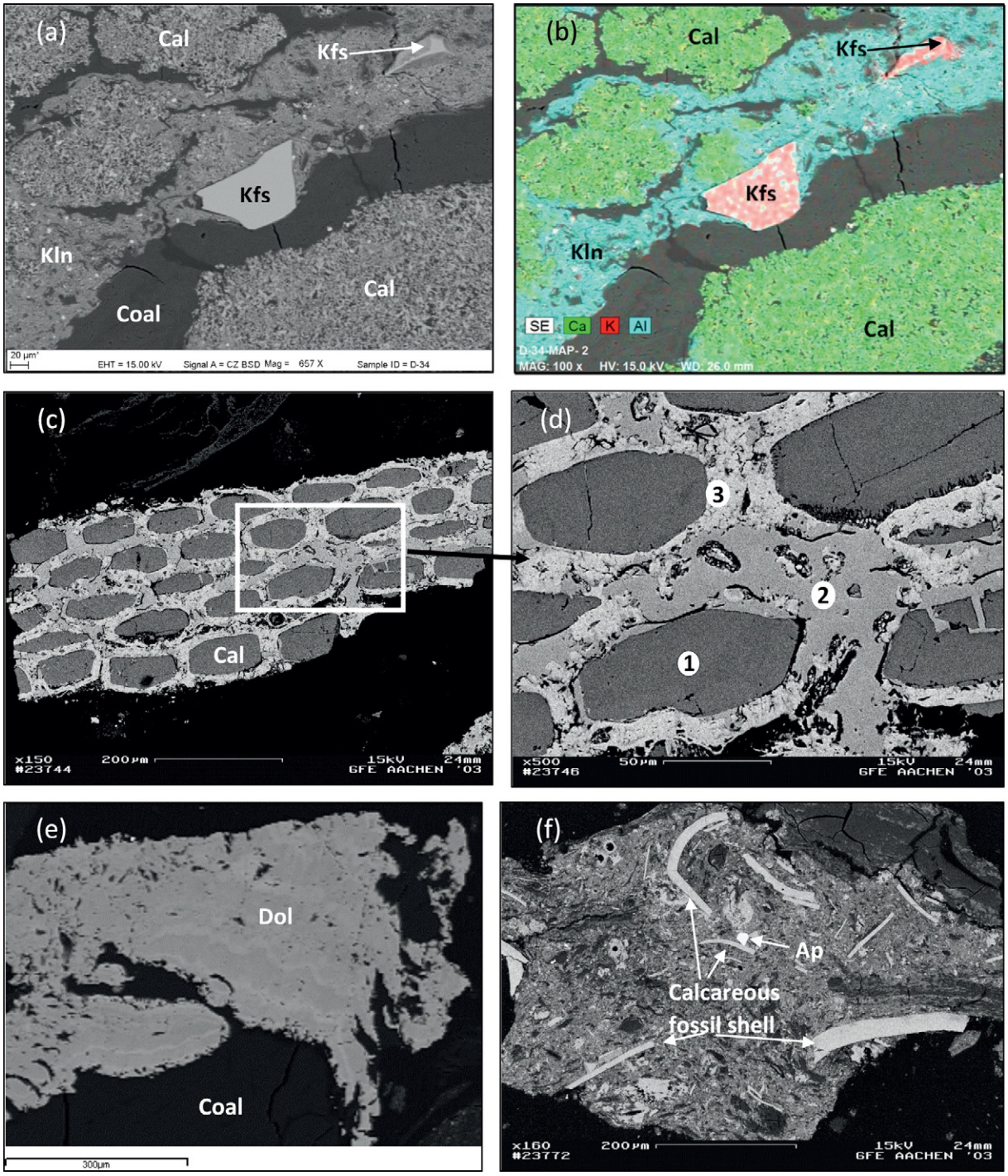

Fig. 9. SEM backscattered images of crystalline phases in the coal samples. a) K-feldspar (Kln) and kaolinite associated with syngenetic calcite (Cal); b) microprobe element mapping of image a; c) calcite (Cal) and replacement carbonates; d) 1: calcite, 2: dolomite and siderite association, 3: calcite and siderite association; e) epigenetic dolomite (Dol); f) calcareous fossil shell remains and apatite (Ap).

The dominance of silicate minerals in bulk coal samples from the kM2 seam and the upper part of the kP1 seam may indicate continuous detrital input into palaeomire. The SEM data shows the presence of individual kaolinite (vermicules?) and as matrices of clay mineral aggregates (Fig. 8a–c). The latter one also contains other minerals (e.g. feldspar, quartz, biotite, apatite, Ti-oxides and zircon) and organic matter. Such clay aggregates are generally related to clastic input from margin (Diessel, 1992; Siavalas et al., 2009). Besides, low ash yields in the kM2 seam along with thin intercalations imply low clastic input during peat accumulation. Thus, clay minerals in the kM2 seam seem to derive rather from another source than from clastic input from pre-Neogene marginal rocks. Individual kaolinite particles and their textures in the coal samples are also similar for kaolinite in tonsteins (Dewison, 1989; Bohor and Triplehorn, 1993; Burger et al., 2000; Dai et al., 2003; Zhao et al., 2012, 2016b; Permana et al., 2013). Therefore, kaolinite and clay aggregates are considered originating from mainly alteration of reworked materials from altered tuff layers and/or clastic inputs from Miocene volcanic rock on the basin margins. Furthermore, apatite, zircon and Ti-oxides are also observed within feldspar crystals; these inclusions also point to clastic input from altered tuff layers/or Miocene volcanic rocks.

Quartz crystals in the studied samples are of variable in size and shape, and mostly identified within clay aggregates; therefore, quartz is of mainly syngenetic (detrital) origin. The cavity-infilling silica is rarely observed in the studied samples, and also cleat-infilling epigenetic silica is determined in few samples from the Eynez sector. It is noteworthy that silica glass shards are also identified through SEM studies, whereas Opal/CT is traced by XRD. The silica shards are generally reported as volcanic input (e.g. air-fall ash) from synchronous volcanic activity (Ruppert and Moore, 1993; Karayiğit et al., 2001; Spears, 2012; Zhao et al., 2012).

Syngenetic authigenic calcite is the most common carbonate mineral (Fig. 3d and 9a), whereas and to a less detrital calcite are observed rarely. Cell- and void-infilling along with replacement carbonates are also commonly identified in samples from the kM2 seam (Fig. 9c and d). Aragonite is commonly reported from Cenozoic coal deposits that contain abundant calcareous fossil remains (e.g. Ward, 1991; Querol et al., 1996; Koukouzas et al., 2010a); however, aragonite is contained either in trace amounts or absent on XRD in similar fossil remains-rich Turkish Neogene coal deposits (Querol et al., 1999; Karayiğit et al., 2001, 2015, 2016; Oskay et al., 2016). It is normal that aragonite can

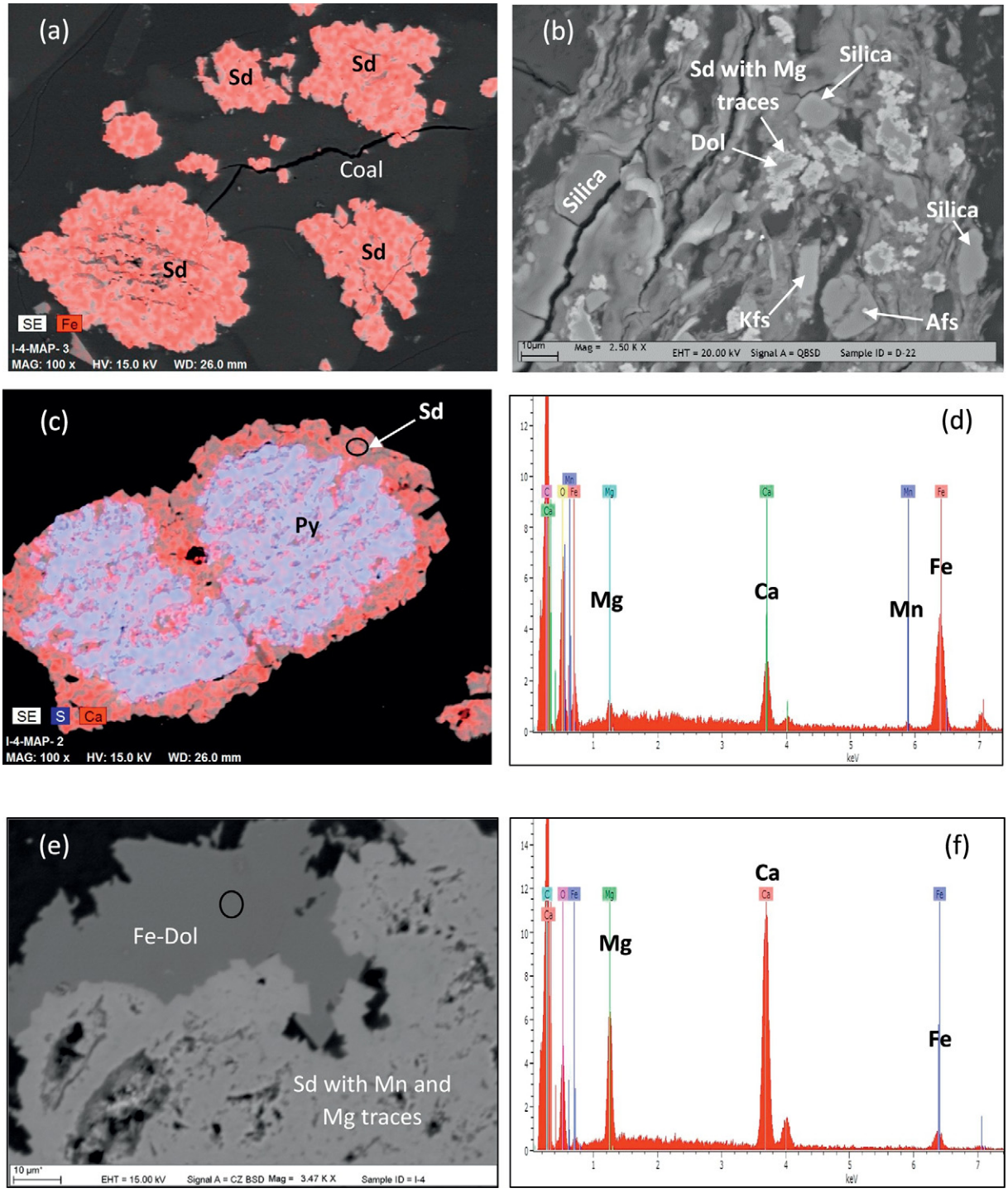

Fig. 10. SEM backscattered images, and selected EDX data and microprobe element mapping of crystalline phases in the coal samples images. a) siderites (Sd) within the cavities of organic matter (telohuminite?); b) siderites (Sd) around dolomites (Dol), and individual silica, K-feldspar (Kfs) and alkali feldspar (Afs) crystals; c) microprobe element mapping of pyrite (Py) and siderite (Sd); e) EDX data for siderite in the image d; e) dolomite (Dol) around siderite (Sd); f) EDX data for dolomite in the image e.

easily convert to calcite in acidic to neutral conditions in the palaeomire and/or during burial; consequently, aragonite is absent and calcite is predominant mineral in most of gastropod-bearing samples in kM3 and kP1 seams. Siderite displays three crystallization types in the studied samples: Mg-and Mn-bearing Ca-siderite (most common), individual siderite nodules with Mn traces, and siderite associated with dolomite (Fig. 10a–f). Siderite in the kP1 seam appears in generally smaller nodules, whereas larger ones are observed in the coal beds of the kM2 seams (Fig. 10a and b). These siderite nodules are presumably related to the low sulphate contents of palaeomire water and Fe derived from the volcanic rocks from the basin margins or altered tuff layers within the coal seam (Dai et al., 2007, 2011; Golab et al., 2013; Ward, 2016; Zhao et al., 2016b); however, the total S contents are slightly high in kM3 and kP1 seams and also siderite is commonly identified around pyrite crystals (Fig. 10c). Therefore, siderite might be formed through reactions between iron and dissolved CO_2 in the palaeomire and the pore water. This can also explain the presence of siderite within maceral cavities (Figs. 3c and 10a). Furthermore, leached water from calcareous intercalations, particularly tuff layers, could penetrate into coal beds during coalification. As a result, reactions between siderite and these solutions, associated with calcite and dolomite took place resulting in the deposition of siderite around pyrites, calcite and/or dolomite (Fig. 10b, c and e).

Pyrite is the only sulphide mineral determined in coal (Table 3); however, other sulphide minerals were identified by SEM-EDX studies (Fig. 8d). Pyrites are mostly represented by syngenetic framboidal crystals and to a lesser extent epigenetic pyrites (e.g. cleat-infillings). Sphalerite and chalcopyrite along with barite are mostly identified in coal beds beneath the tuff layers and this observation suggests that these were formed from precipitation of leachates from those tuff layers (Fig. 8d and f). Gypsum was presumably formed in the pores from water evaporation during storage of the coal samples.

4.6. Elemental composition

The major elements (≥1000 ppm) in the three seams are Al, Ca, Fe, K, Mg and Na (Table 4). The B, P and Ti concentrations can reach >1000 ppm in some coal samples (Table 4), whereas Ba, Sr, V and Zn are variable in the three seams exceeding 100 ppm in certain coal samples. In addition, the Mn concentration exceeds 100 ppm in kM2 and kP1 seams. The concentrations of trace elements are mostly below 10 ppm; however, As and Zr contents exceed 100 ppm in some coal beds beneath the tuff layers. Previous studies also reported similar elemental concentrations in the feeding coal from the Soma Basin (Karayiğit et al., 2000, 2006; Tuncalı et al., 2002). The vertical elemental distribution varies from seam to seam. The major elements (Al, Fe, K, Mg and Na), and most of minor (e.g. Ba, P, Ti) and trace elements (e.g. Cu, Zn) show increasing trends upwards in the kP1 seam, whereas Ca, As and Mo a decreasing one. In contrast, elemental contents tend to decrease towards the upper parts in the kM2 and kM3 seams. Boron in the kM2, and Mo and Ba in the kM3 seam display increasing trends upwards. These changes are mostly similar to the vertical distributions of ash yield in the seams pointing to an inorganic affinity of these elements. The weighted averages of elements in each sector are variable and elemental enrichments are generally changeable (Table 4). Nevertheless, the elements Cs, Li and U are enriched in almost all the studied coal seams in comparison with most world coals (Swaine, 1990). In the Deniş sector, B, Cd, Li and V are enriched in both kM2 and kP1 seams, and Ti, Cr, and Th are only enriched in the kP1 seam. The elemental concentrations, beside U, in the kM2 seam at the Işıklar sector are within the averages of most world coals. Furthermore, the concentrations of several minor and trace elements in the three coal seams show higher average values than the world low-rank coals (Ketris and Yudovich, 2009).

5. Discussion

5.1. Hydrocarbon source potential

Humic coals with high vitrinite/huminite contents and liptinite contents exceeding 10–15% (on mineral matter-free basis) are generally considered as oil-prone (Hunt, 1991; Wilkins and George, 2002). Nevertheless, the oil generation potential of humic coals is a complex case. Several parameters and diagrams have been proposed for an accurate approach (Pepper and Corvi, 1995; Killops et al., 1998; Sykes and Snowdon, 2002; Petersen, 2006). The huminite and liptinite contents along with the thickness of the coal beds might suggest a possible HC-generation potential (Table 1, Fig. 2), which is firstly evaluated on the basis of the HI vs. OI and HI vs. T_{max} diagrams (Fig. 4). The samples are projected on the mainly oil and mixed hydrocarbon generation window on the HI vs. OI diagram; however, all samples are plotted on gas-prone area on HI vs. T_{max} diagram. This plotted data are related to the predominance of type III kerogen (huminite macerals) in the studied samples. The occurrence of exsudanite in some samples can also suggest the development of early petroleum generation and the mixed hydrocarbon generation potential for certain coal beds in the Soma Basin. Samples with HI lower than 150 mg HC/g TOC are generally considered as gas-prone (Hunt, 1991; Peters and Moldowan, 1993; Petersen, 2006); thus, the studied coal samples are more gas-prone rather than mixed generation potential. In addition, several studies also suggest that HI values are not accurate for humic coals to estimate the true generation potential (Petersen, 2006; and refs. therein), and calculated HI_{max} values (or "effective HI" according to Sykes and Snowdon, 2002) on HI vs. VR plot could be more accurate for initial hydrocarbon potential. The calculated HI_{max} values are within the range for gas- and oil-prone coals (Fig. 5); and none of sample reach required HI_{max} value (300 mg HC/g TOC) for oil generation (Fig. 11). Considering this along with R_o (≤0.50%), low PI, BI and QI values (see Table 1) the coal beds in the studied sectors are generally gas-prone.

5.2. Mode of occurrence of elements

The existences of potentially hazardous trace elements in coal and their modes occurrences have been studied widely during last three decades. Several methods were developed and the most commonly applied one is statistical and as well selective leaching methods. Even though some objections are existed for the accuracy of the statistical methods (Drew et al., 2008; Geboy et al., 2013); the statistical methods

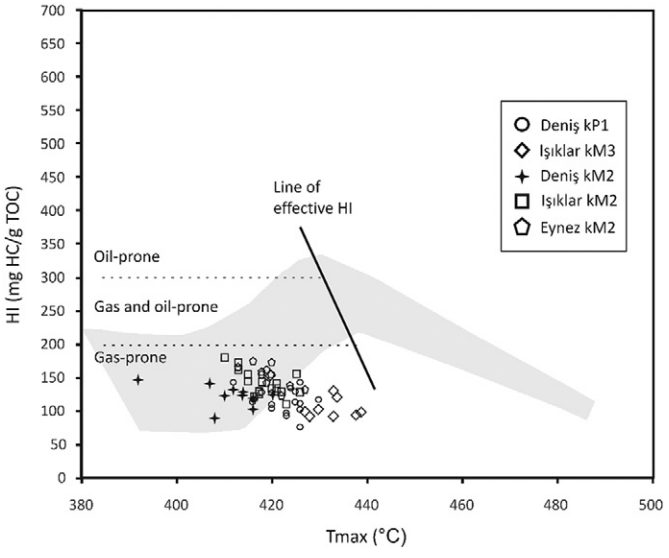

Fig. 11. Plot of HI vs. T_{max} of Soma coal (after Sykes and Snowdon (2002)).

can be more effective when it is accompanied by direct methods such as SEM-EDX (Eskanazy et al., 2010 and ref. therein). Thus, in the recent study statistical analysis was also supported by the SEM-EDX data. The kM2 seam displays generally lower elemental concentrations and ash yields; in contrast, higher elemental concentrations and ash yields are recorded from the kP1 seam (Table 4). Therefore, almost all elements display strong positive correlations to ash yield and strong negative correlation to TOC content (Table 5). All this suggests that the majority of elements mostly have inorganic affinity. Nevertheless, no significant correlation between ash yield and Ca, As, B, Mo, W and U is recorded. Thus, these elements seem to have an intermediate affinity.

The major elements Al, Fe, K, Mg and Na show strong positive correlations with most of minor and trace elements (Table 5). Considering these correlations along with the common presence of aluminosilicate minerals, Al, Fe, K, Mg and Na and associated elements (e.g. Co, Cr, Li and Zr) seem being mainly affiliated with clay minerals and/or feldspars in coal. Therefore, clastic input from volcanic rocks on the basin margins might have been the main source of major and aluminosilicate-affiliated elements. Similar cases are also reported from coal deposits that adjacent area host synchronous volcanic rocks and as well altered volcanic matter or tonstein-bearing coal seams (Querol et al., 1997; Zhou et al., 2000; Dai et al., 2003, 2007, 2010; Li et al., 2017; Zhao et al., 2012, 2017). Calcium displays only a weak correlation with Sr and this association could be related to the existence of carbonate minerals. Furthermore, the SEM-EDX data shows that Fe, Mg and Mn partly distribute in carbonate minerals, particularly siderite (Fig. 10d and f), whereas Ca is also traced on organic matter explaining its intermediate affinity and the weak correlation to Sr. The correlation between Ca and Sr can be related to the presence of gastropod fossil-shell remains (Querol et al., 1996; Karayiğit et al., 2000, 2001). Moreover, the traceable Ca and as well as S in organic matter are probably related to dissolved ions of these elements in the pore water that can be bounded with organic matter (Ward, 1991; Li et al., 2007, 2010; Dai et al., 2015b; Ward, 2016; Karayiğit et al., 2017).

Table 5
Elemental affinities deduced from the calculation of Pearson's correlation coefficients.

Correlation with ash yield (0.70 < r < 1.0)
Al, K, Fe, Mg, Bi, Ce, Cu, Co, Cr, Cs, Dy, Er, Eu, Ga, Gd, Hf, Ho, La, Li, Lu, Nb, Nd, Ni, Pb, Pr, Rb, Sc, Sm, Sn, Ta, Tb, Th, Ti, Tm, Y, Yb, Zr
Correlation with ash yield (0.50 < r < 0.70)
Na, Cs, Cd, Ni, Ge, Pb, Sb, Tl, V, Zn
Correlation with Al content (0.70 < r < 1.0)
Fe, K, Mg, Be, Bi, Ce, Cu, Co, Cr, Dy, Er, Eu, Ga, Gd, Hf, Ho, La, Li, Lu, Nb, Nd, Ni, Pr, Pb, Rb, Sc, Sm, Sn, Ta, Tb, Th, Ti, Tm, V, Y, Yb, Zn, Zr
Correlation with Al content (0.50 < r < 0.7)
Na, Cd, Cs, Ge, Sb, Tl
Correlation with Fe content (0.70 < r < 1.0)
K, Be, Bi, Ce, Cu, Co, Cr, Dy, Er, Eu, Ga, Gd, Hf, Ho, La, Li, Nb, Nd, Pb, Pr, Sm, Sn, Ta, Tb, Th, Ti, Tm, Y, Zr
Correlation with Fe content (0.50 < r < 0.70)
Mg, Cs, Ge, Ni, Rb, Sb, Sc, Tl, V
Correlation with Ca content
Sr (0.43)
Correlation with K content (0.70 < r < 1.0)
Mg, Be, Bi, Ce, Cu, Co, Cr, Dy, Er, Eu, Ga, Gd, Hf, Ho, La, Li, Lu, Nb, Nd, Ni, Pb, Pr, Rb, Sc, Sm, Sn, Ta, Tb, Th, Ti, Tm, V, Y, Yb, Zn, Zr
Correlation with K content (0.50 < r < 0.70)
Na, Cs, Ge, Sb, Tl
Correlation with Mg content (0.70 < r < 1.0)
Be, Bi, Ce, Dy, Er, Eu, Ga, Gd, Hf, Ho, La, Lu, Nb, Nd, Pb, Pr, Rb, Sm, Sn, Ta, Tb, Th, Ti, Tm, Y, Yb, Zr
Correlation with Mg content (0.50 < r < 0.70)
Cr, Co, Cu, Li, Ni, Sc, V, Zn
Correlation with Na content (0.50 < r < 1.0)
Be, Bi, Ce, Dy, Er, Eu, Ga, Gd, Ho, La, Nb, Nd, Pb, Pr, Rb, Sm, Sn, Ta, Th, Tm, Y, Tb, Zn

The SEM-EDX data also denotes that minor and trace elements could have rather another mineral affinity beyond aluminosilicates. The clay mineral aggregates associated with accessory minerals such as zircon, chromite, apatite and monazite, are sources for Zr, P and Cr along with the REEs in the studied samples. The geochemical analyses from volcanic rocks on the basin margins show the presence of Ba, Cr, Ni, Sr, Zr, Th, U and REEs as well (Ersoy et al., 2012). This is evidence that most of minor and trace elements mostly derive from clastic input and explain the relatively high concentrations of U, Zr and REEs in some coal samples above the altered tuff layers in the kM2 seam (Crowley et al., 1989; Hower et al., 1999; Dai et al., 2006a; Dai et al., 2013) Barite could also be the source for Sr (Fig. 8f). Furthermore, the accessory monazite minerals could also be source for REE elements and as well Th in the studied samples. The elements As, Cu, Pb and Zn are commonly traced in sulphide minerals (Fig. 8e); as previously mentioned they generally display higher concentrations beneath the tuff layers. This implies that leachates from tuff layers precipitated within the coal beds during late diagenetic stages (Querol et al., 1997; Dai et al., 2006a; Dai et al., 2007). Thus, epigenetic sulphide minerals could cause the As, Cu and Zn enrichments in the kM2 and kP1 seams. The synchronous volcanic activity also caused B enrichments in most Turkish coals (Querol et al., 1997; Karayiğit et al., 2000). Surface waters leaching volcanic rocks on the basin margins and tuff layers within the basin could bring B-rich water into palaeomires in the Soma Basin. Thus, B could uptake by either peat-forming plants or adsorbed by clay minerals. This could explain the intermediate affinity of B in the studied coal samples. Another element can be introduced by the surface waters leaching is U and, as like B, it could be absorbed by clay minerals and/or uptake by peat-forming plants (Querol et al., 1996; Dai et al., 2011). Thus, B and U display intermediated affinity in the studied samples.

5.3. Coal facies indices

The coal maceral diagrams, if combined with mineralogical, sedimentological, palaeontological and geochemical data, could be a useful tool providing information about depositional conditions within the palaeomire (Siavalas et al., 2009; Bechtel et al., 2014; Karayiğit et al., 2015, 2016; Oikonomopoulos et al., 2015). The widely used ternary diagram proposed by Mukhopadhyay (1989), provides information about depositional conditions and common vegetation during peat accumulation. Fig. 12 indicates that precursor peat of the kM2 seam accumulated under slight anoxic conditions, and watertable was high and stable. Forested fen was common and tissues were well preserved. In contrast, watertable was unstable during peat accumulation of the kM3 and kP1 seams. The dominant vegetation in these seams was herbaceous, particularly reed plants. The upper part of the kM3 seam at Işıklar sector displays more oxic conditions and inertinite content is higher than in other samples of kM2 seam from the same sector. This difference might be related with either drier conditions in this part of the basin or a masking effect from high allochthonous inertinite input. The latter one seems to be more possible due to predominance of inertodetrinite embedded within densinite. Such association generally points to rather allochthonous origin for inertinite than oxidation (O'Keefe et al., 2013).

The differences between seams are more distinct on the Tissue Preservation Index (TPI) vs. Gelification Index (GI) and Groundwater Influence (GWI) vs. Vegetation Index (VI) diagrams (Fig. 13). The kM2 seam is characterized by high to very high TPI (1.5–16), VI (0.8–5.6), and moderate to high GI (2.2–67.9) values (Fig. 13a and b). TPI-GI values similar to these of kM2 seam are generally reported from xylite-bearing Neogene coal formed in wet forest mire conditions (Kolcon and Sachsenhofer, 1999; Kalaitzidis et al., 2004; Oikonomopoulos

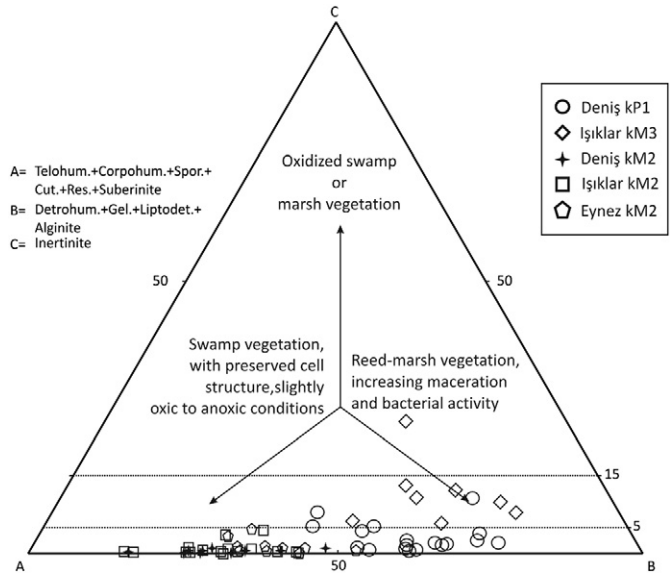

Fig. 12. ABC ternary plot of the coal samples from sampling profile (after Mukhopadhyay (1989)).

et al., 2015). The fossilized wood trunks and branches in the kM2 seam are further evidence for the predominance of woody vegetation and wet-forest mire conditions. The organic geochemical results also reveal the high-plant contribution and previous palynological studies also imply the dominance of woody vegetation in the basin (Nebert, 1978; Akgün et al., 1986; Gemici et al., 1991). The wet conditions during the kM2 seam could be related to humid climate during late Early to Middle Miocene in western Turkey (Kayseri-Özer, 2017). The GWI values of the kM2 seam could be interpreted as low water table conditions (Fig. 13b). Nevertheless, these low GWI values are characteristic for the Cenozoic xylite-rich coals (Kalaitzidis et al., 2004; Koukouzas et al., 2010b; Oikonomopoulos et al., 2015; Mitrović et al., 2016). The low TPI (<1.0) and VI (<1.0), and low to moderate GI (0.8–25.4) and GWI (1.6–11.1) values from kM3 and kP1 seams indicate predominance of herbaceous vegetation and fluctuated watertable during peat accumulation (Fig. 13a and b). The *n*-alkane distribution pattern of analysed samples from the kP1 seam also indicates the predominance of the herbs (e.g. macrophytes) in the palaeomire (see Fig. 6d). The vegetation difference is presumably related to climatic changes in the Soma Basin during Miocene. Furthermore, moderate to high GI values in all three seams could be related to Ca-rich water influence in the Basin in which allowed the development of alkaline conditions and biochemical gelification within the paleomire (Querol et al., 1996; Oikonomopoulos et al., 2015).

5.4. Depositional environment

The coal facies, lithological and mineralogical data imply that the depositional environment was changeable during the Soma Formation deposition. The seam comprises thick coal beds with thin inorganic intercalations also suggesting high and stable water table and low

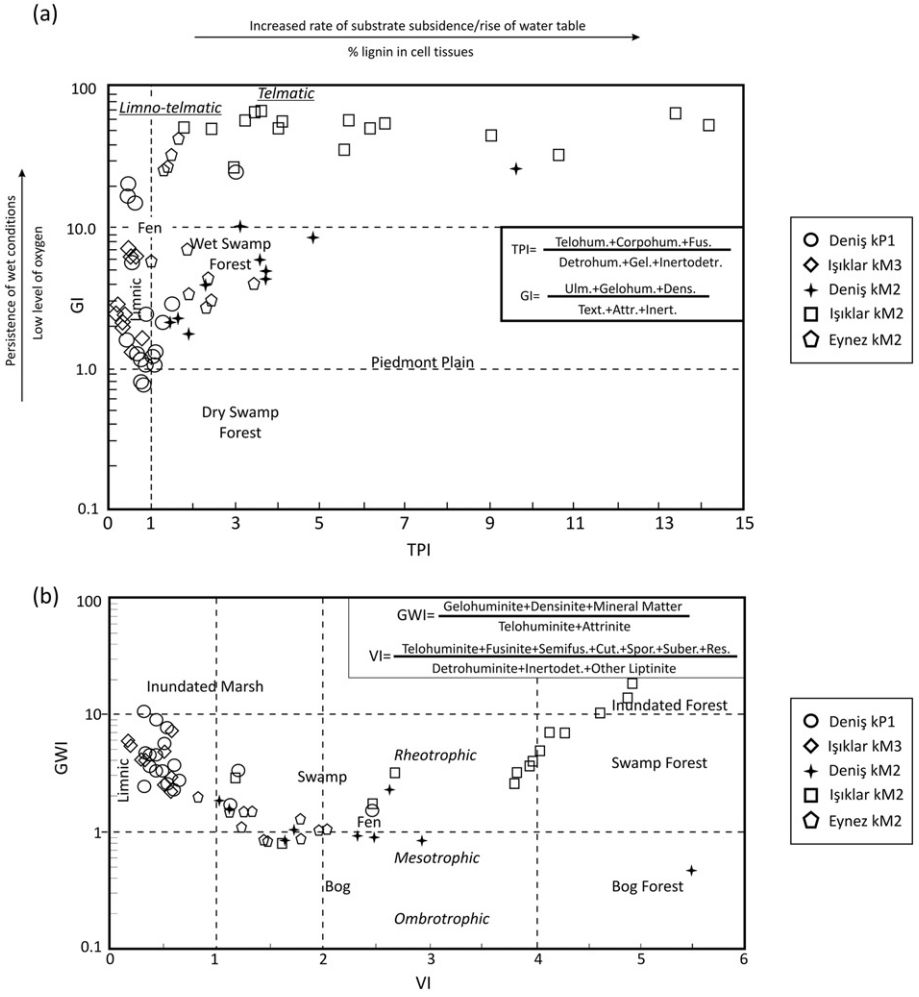

Fig. 13. a) GI vs. TPI plot of the coal samples from sampling profile (after Diessel (1992), as modified by Kalaitzidis et al. (2004)); b) VI vs. GWI plot of the coal samples from sampling profile (after Calder et al. (1991), as modified by Kalaitzidis et al. (2004)).

clastic input. Therefore, coal samples of the kM2 seam display low concentrations of aluminosilicate-affiliated elements and TOC values are high. In addition, low energy conditions allowed precipitation of siderite nodules in the palaeomires (Oikonomopoulos et al., 2008) and their coexistence with other syngenetic carbonates and pyrites also imply neutral to weak alkaline conditions during peat accumulation. Furthermore, predominance of woody vegetation and good preservation conditions are generally related to high HI values (Collinson et al., 1994; Petersen et al., 2009); this relation might explain slightly higher HI and TOC values in the kM2 seam (see Table 1). The common presences of the altered tuff layers and thin intercalations in the kM2 seam suggest the peat accumulation seems to have been ceased mainly by regional volcanic activity during Early to Middle Miocene;

The clayey limestone/marl previously identified as a marl series by İnci (1998a, 2002), forms the roof of the kM2 seam. This unit is related to the development of deeper conditions and/or lake expansion in the Soma Basin as a result of vertical tectonic movements. Furthermore, the presence of clay minerals in this unit also indicates that the clastic fluvial material was also entered the palaeomire during this period of time. Under shallow water conditions the precursor peat of kM3 seam begun accumulating but this process was ceased several times, and calcareous intercalations were deposited (see Fig. 2). This alteration between coal beds and calcareous intercalations could indicate vertical tectonic movements that presumably activated karstic aquifer in the marginal areas resulting in a rise of water table. The common presence of carbonate minerals and fossil fragments in the kM3 seam may indicate that Ca-rich water discharge were developed, and alkaline conditions were also common in the palaeomire (Querol et al., 1996; Bechtel et al., 2004; Siavalas et al., 2009; Karayiğit et al., 2015). The presence of syngenetic pyrite in this seam also implies the influence of sulphate-rich water into the palaeomire and the development of neutral to weak alkaline conditions. The development of slightly alkaline conditions also allows the bacterial activity that could reduce tissue preservation; this also explains the relatively low TOC and TPI values in this seam. These values might also be related to the predominance of herbaceous vegetation in the palaeomire. Overall, the precursor peat in the Soma Formation started to accumulated under pure telmatic conditions at the early stages (kM2 seam), whereas limno-telmatic conditions were more dominant at late stages of peat accumulation (kM3 seam).

At the start of the Late Miocene, fluvial conditions became again dominant; later on they turned to limnic where precursor peat of the kP1 seam was accumulated. The differences on mineralogical, lithological and maceral compositions of coal beds throughout the kP1 seam suggest changes of water chemistry and clastic input in the palaeomire during the Late Miocene. The lower part was presumably deposited under alkaline conditions and low clastic input that allowed the formation of syngenetic carbonates. The predominance of silicates along with high ash yields in the upper part implies tectonic movements and high clastic input into the basin. Noteworthy, clayey bands and silicate minerals are dominant above the altered tuff layer in the kP1 seam indicating that the clastic input from basin margins was increased after the volcanic activity during the Late Miocene. The increased clastic input along with the alkaline conditions could also reduce preservation of organic matter that resulted in lower TOC values in this seam. All these denote that peat was accumulating under limno-telmatic conditions, whereas fluvial and volcanoclastic inputs ceased peat formation several times during the Late Miocene.

6. Conclusions

The alternations between alluvial-fluvial-lacustrine conditions imply that the Soma Graben was activated several times during the Miocene as a result of the regional extensional tectonic regime. This regime along with climatic factors controlled peat-forming environment in the Soma Basin. The palaeomire in the Soma Basin commenced to develop under pure telmatic and low energy conditions; peat-forming vegetation was dominated by woody species. These conditions resulted in the formation of thick beds of low-ash and high TOC coal in the kM2 seam. In the subsequent periods, watertable was fluctuating and cover the entire mire surface several times; thus, peat formation ceased resulting in the deposition of clastic and calcareous intercalations in kM3 and kP1 seams. The lithological and mineralogical features of these intercalations indicate the development of limno-telmatic conditions with fluvial contributions and also the water supplied the palaeomire was presumably Ca-rich shifting to more alkaline conditions during accumulation of precursor peat of the kM3 and kP1 seams. Therefore, coal of kM3 and kP1 seams display relatively high total S contents and low TOC values than the kM2 seam. The regional volcanic activities took place during the kM2 and kP1 peat accumulation; hence, several tuff layers are hosted in these seams. The mineralogical composition of these layers also point to felsic volcanic activity around the Soma Basin; their composition is similar to tonstein.

The results of the pyrolysis analysis of the coal samples are in agreement with maceral composition and rank. The kerogen type-III is common in all the seams and low OI values in the kM3 are related to slightly high inertinite values. The HI and T_{max} values suggest that kM2 and kM3 coal is immature to early mature and kP1 coal is clearly immature. Furthermore, the vegetation changes during Miocene in the Soma Basin are also reflected on the HI values. The slightly higher HI in the kM2 coal seems to be related to high contributions of the woody material in peat and development of more acidic conditions during peat accumulation, whereas relative low HI values in kM3 and kP1 coal are related to contributions of herbaceous plants and more alkaline conditions. Even though, the thickness of coal beds along with high huminite and liptinite contents of the coal samples can suggest the oil generation potential, the pyrolysis analysis data shows that the studied coal seams are mainly gas-prone and only certain coal beds display mixed hydrocarbon generation capacity. All these suggest that the features of coal seams in the Soma Basin were controlled by changes in the depositional conditions and vegetation during the Neogene times.

Acknowledgements

This study was supported by Hacettepe University Scientific Research Coordination Unit. Project Numbers: 00.02.602.005 and FAY-201-10601.The authors would to thank Prof. Dr. İsmail Hakkı Demirel (Hacettepe University), Asst. Prof. Dr. İbrahim Buzkan (Bülent Ecevit University), and Dr. Maria Mastalerz (Indiana University) for their assistance and suggestions during the project implementation. The first author also thanks the German Academic Exchange Service (DAAD) for funding the research visits to Germany. Finally, Dr. Shifeng Dai, Editor-in-Chief of the Journal, and anonymous reviewers are thanked for their comments and suggestions.

References

Akgün, F., 1993. Palynological age revision of the Neogene Soma coal basin. Bull. Geol. Soc. Greece 28, 151–170.
Akgün, F., Alişan, C., Akyol, E., 1986. A palynological approach to the Neogene stratigraphy of Soma area. Geol. Soc. Turk. Bull. 29, 13–25.
American Society for Testing and Materials (ASTM) D3174, 2012. Standard Test Method for Ash in the Analysis Sample of Coal and Coke from Coal. ASTM International, West Conshohocken, PA (6 pp).
American Society for Testing and Materials (ASTM) D3175, 2011. Standard Test Method for Volatile Matter in the Analysis Sample of Coal and Coke. ASTM International, West Conshohocken, PA (6 pp).
American Society for Testing and Materials (ASTM) D3302, 2015. Standard Test Method for Total Moisture in Coal. ASTM International, West Conshohocken, PA (8 pp).
American Society for Testing and Materials (ASTM) D5373, 2016. Standard test methods for determination of carbon. Hydrogen and Nitrogen in Analysis Samples of Coal and Carbon in Analysis Samples of Coal and Coke. ASTM International, West Conshohocken, PA (11 pp).
American Society for Testing and Materials (ASTM) D5865, 2013. Standard Test Method for Gross Calorific Value of Coal and Coke. ASTM International, West Conshohocken, PA (19 pp).

Arbuzov, S.I., Mezhibor, A.M., Spears, D.A., Ilenok, S.S., Shaldybin, M.V., Belaya, E.V., 2016. Nature of tonsteins in the Azeisk deposit of the Irkutsk Coal Basin (Siberia, Russia). Int. J. Coal Geol. 153, 99–111.

Baysal, M., Yürüm, A., Yıldız, B., Yürüm, Y., 2016. Structure of some western Anatolia coals investigated by FTIR, Raman, ^{13}C solid state NMR spectroscopy and X-ray diffraction. Int. J. Coal Geol. 163, 166–176.

Bechtel, A., Markic, M., Sachsenhofer, R.F., Jelen, B., Gratzer, R., Lücke, A., Püttmann, W., 2004. Paleoenvironment of the upper Oligocene Trbovlje coal seam (Slovenia). Int. J. Coal Geol. 57, 23–48.

Bechtel, A., Karayiğit, A.İ., Sachsenhofer, R.F., İnaner, H., Christanis, K., Gratzer, R., 2014. Spatial and temporal variability in vegetation and coal facies as reflected by organic petrological and geochemical data in the Middle Miocene Çayirhan coal field (Turkey). Int. J. Coal Geol. 134–135, 46–60.

Bechtel, A., Karayiğit, A.I., Bulut, Y., Mastalerz, M., Sachsenhofer, R.F., 2016. Coal characteristics and biomarker investigations of Dombayova coals of Late Miocene-Pliocene age (Afyonkarahisar-Turkey). Org. Geochem. 94, 52–67.

Benda, L., 1971. Principles of the palynologic subdivision of the Turkish Neogene. Newsl. Stratigr. 23–26.

Bohor, B.F., Triplehorn, D.M., 1993. Tonstein: altered volcanic ash layers in coal-bearing sequences. Geol. Soc. Am. Spec. Pap. 285, 40.

Bulut, Y., Karayiğit, A.İ., 2006. Petrography of feed coals in the Soma power plant, Manisa, Turkey. Energy Sources A 28, 1447–1459.

Burger, K., Bandelow, F.K., Bieg, G., 2000. Pyroclastic kaolin coal–tonsteins of the Upper Carboniferous of Zonguldak and Amasra, Turkey. Int. J. Coal Geol. 45, 39–53.

Burger, K., Zhou, Y., Ren, Y., 2002. Petrography and geochemistry of tonsteins from the 4th Member of the Upper Triassic Xujiahe formation in Southern Sichuan Province, China. Int. J. Coal Geol. 49, 1–17.

Calder, J., Gibling, M., Mukhopadhyay, P., 1991. Peat formation in a Westphalian B piedmont setting, Cumberland Basin, Nova Scotia. Bull. Soc. Géol. Fr. 162, 283–298.

Canuel, E., Freeman, K., Wakeham, S., 1997. Isotopic compositions of lipid biomarker compounds in estuarine plants and surface sediments. Limnol. Oceanogr. 42, 1570–1583.

Collinson, M.E., Van Bergen, P.F., Scott, A.C., De Leeuw, J.W., Scott, A.C., Fleet, A.J., 1994. The oil-generating potential of plants from coal and coal-bearing strata through time: a review with new evidence from carboniferous plants. Coal and Coal-bearing Strata as Oil-prone Source Rocks? 77. Geol. Soc. London, pp. 31–70 (Spec. Publ.).

Creech, M., 2002. Tuffaceous deposition in the Newcastle Coal Measures: challenging existing concepts of peat formation in the Sydney Basin, New South Wales, Australia. Int. J. Coal Geol. 51, 185–214.

Crowley, S.S., Stanton, R.W., Ryer, T.A., 1989. The effects of volcanic ash on the maceral and chemical composition of the C coal bed, Emery Coal field, Utah. Org. Geochem. 14, 315–331.

Dai, S., Ren, D., Hou, X., Shao, L., 2003. Geochemical and mineralogical anomalies of the late Permian coal in the Zhijin Coalfield of southwest China and their volcanic origin. Int. J. Coal Geol. 55, 117–138.

Dai, S., Ren, D., Chou, C.-L., Li, S., Jiang, Y., 2006a. Mineralogy and geochemistry of the no. 6 coal (Pennsylvanian) in the Junger coalfield, Ordos Basin, China. Int. J. Coal Geol. 66, 253–270.

Dai, S., Zhou, Y., Ren, D., Wang, X., Li, D., Zhao, L., 2007. Geochemistry and mineralogy of the Late Permian coals from the Songzo Coalfield, Chongqing, southwestern China. Sci. China Earth Sci. 50, 678–688.

Dai, S., Wang, X., Chen, W., Li, D., Chou, C.-L., Zhou, Y., Zhu, C., Li, H., Zhu, X., Xing, Y., Zhang, W., Zou, J., 2010. A high-pyrite semianthracite of Late Permian age in the Songzao Coalfield, southwestern China: mineralogical and geochemical relations with underlying mafic tuffs. Int. J. Coal Geol. 83, 430–445.

Dai, S., Wang, X., Zhou, Y., Hower, J.C., Li, D., Chen, W., Zhu, X., Zou, J., 2011. Chemical and mineralogical compositions of silicic, mafic, and alkali tonsteins in the late Permian coals from the Songzao Coalfield, Chongqing, Southwest China. Chem. Geol. 282, 29–44.

Dai, S., Zhang, W., Ward, C.R., Seredin, V.V., Hower, J.C., Li, X., Song, W., Wang, X., Kang, H., Zheng, L., Wang, P., Zhou, D., 2013. Mineralogical and geochemical anomalies of Late Permian coals from the Fusui Coalfield, Guangxi Province, southern China: influences of terrigenous materials and hydrothermal fluids. Int. J. Coal Geol. 105, 60–84.

Dai, S., Li, T., Seredin, V.V., Ward, C.R., Hower, J.C., Zhou, Y., Zhang, M., Song, X., Song, W., Zhao, C., 2014. Origin of minerals and elements in the Late Permian coals, tonsteins, and host rocks of the Xinde Mine, Xuanwei, eastern Yunnan, China. Int. J. Coal Geol. 121, 53–78.

Dai, S., Li, T., Jiang, Y., Ward, C.R., Hower, J.C., Sun, J., Liu, J., Song, H., Wei, P., Li, Q., Xie, P., Huang, Q., 2015a. Mineralogical and geochemical compositions of the Pennsylvanian coal in the Hailiushu Mine, Daqingshan Coalfield, Inner Mongolia, China: implications of sediment-source region and acid hydrothermal solutions. Int. J. Coal Geol. 137, 92–110.

Dai, S., Liu, J., Ward, C.R., Hower, J.C., Xie, P., Jiang, Y., Hood, M.M., O'Keefe, J.M.K., Song, H., 2015b. Petrological, geochemical, and mineralogical compositions of the low-Ge coals from the Shengli Coalfield, China: a comparative study with Ge-rich coals and a formation model for coal-hosted Ge ore deposit. Ore Geol. Rev. 71, 318–349.

Dewison, M.G., 1989. Dispersed kaolinite in the Barnsley Seam coal (U.K.): evidence for a volcanic origin. Int. J. Coal Geol. 3-4, 291–304.

Diessel, C.F.K., 1992. Coal-bearing Depositional Systems. Springer, Berlin (721 pp).

Drew, L., Grunsky, E., Schuenemeyer, J., 2008. Investigation of the structure of geological process through multivariate statistical analysis–the creation of a coal. Math. Geosci. 40, 789–811.

Economic Commission for Europe — United Nations (E.C.E. — U.N.), 1998. International classification of in-seam coals. ECE, Energy/19 (Geneva).

Ersoy, E., Dindi, F., Karaoğlu, O., Helvacı, C., 2012. Geochemical and petrographic features of the Miocene volcanism around Soma Basin, Western Anatolia, Turkey. Yerbilimleri 33, 59–80 (in Turkish with English abstract).

Escobar, M., Márquez, G., Suárez-Ruiz, I., Juliao, T.M., Carruyo, G., Martínez, M., 2016. Source-rock potential of the lowest coal seams of the Marcelina Formation at the Paso Diablo mine in the Venezuelan Guasare Basin: evidence for the correlation of Amana oils with these Paleocene coals. Int. J. Coal Geol. 163, 149–165.

Eskanazy, G., Finkelman, R.B., Chattarjee, S., 2010. Some considerations concerning the use of correlation coefficients and cluster analysis in interpreting coal geochemistry data. Int. J. Coal Geol. 83, 491–493.

Espitalié, J., Laporte, J.L., Madec, M., Marquis, F., Leplat, P., Paulet, J., Boutefeu, A., 1977a. Méthode rapide de caractérisation des roches mères de leur potentiel pétrolier et de leur degré d'évolution. Revue de L'Institut Français du Pétrole 32, 23–42.

Espitalié, J., Madec, M., Tissot, B., 1977b. Source rock characterization method for petroleum exploration. Proceedings 9th Offshore Technology Conference. vol. 3. Offshore Technology Conference, Houston, pp. 439–444.

Ficken, K.J., Li, B., Swain, D.L., Eglinton, G., 2000. An n-alkane proxy for the sedimentary input of submerged/floating freshwater aquatic macrophytes. Org. Geochem. 31, 745–749.

Gemici, Y., Akyol, E., Akgün, F., Seçmen, Ö., 1991. Macro and micro fossil flora of Soma coal area. Bull. Min. Res. Expl. 112, 161–178 (in Turkish with English abstract).

Geboy, N.J., Engle, M.A., Hower, J.C., 2013. Whole-coal versus ash basis in coal geochemistry: a mathematical approach to consistent interpretations. Int. J. Coal Geol. 113, 41–49.

Ghazwani, A.A., Littke, R.A., Sachse, V.A., Fink, R.A., Mahlstedt, N.B., Hartkopf-Fröder, C.C., 2016. Organic geochemistry, petrology and palynofacies of Middle Devonian lacustrine flagstones in the Orcadian Basin, Scotland: depositional environment, thermal history and petroleum generation potential. Geol. Mag. http://dx.doi.org/10.1017/S0016756816000984.

Golab, A., Ward, C.R., Permana, A., Lennox, P., 2013. High-resolution three-dimensional imaging of coal using microfocus X-ray computed tomography, with special reference to modes of mineral occurrence. Int. J. Coal Geol. 113, 97–108.

Grevenitz, P., Carr, P., Hutton, A., 2003. Origin, alteration and geochemical correlation of Late Permian airfall tuffs in coal measures, Sydney Basin, Australia. Int. J. Coal Geol. 55, 27–46.

Gross, D., Bechtel, A., Harrington, G.J., 2015. Variability in coal facies as reflected by organic petrological and geochemical data in Cenozoic coal beds offshore Shimokita (Japan) - IODP Exp.337. Int. J. Coal Geol. 152, 63–79.

Hokerek, S., Ozcelik, O., 2015. Organic facies characteristics of the Miocene Soma Formation (Lower Lignite Succession-KM2), Soma Coal Basin, western Turkey. Energy Procedia 76, 27–32.

Hower, J.C., Ruppert, L.F., Eble, C.F., 1999. Lanthanide, yttrium, and zirconium anomaliesin the fire Clay coal bed, Eastern Kentucky. Int. J. Coal Geol. 39, 141–153.

Hunt, J.M., 1991. Generation of gas and oil from coal and other terrestrial organic matter. Org. Geochem. 17, 673–680.

İnci, U., 1998a. Lignite and carbonate deposition in middle lignite succession of the Soma Formation, Soma coalfield, western Turkey. Int. J. Coal Geol. 37, 287–313.

İnci, U., 1998b. Miocene synvolcanic alluvial sedimentation in Lignite-bearing Soma Basin, Western Turkey. Turk. J. Earth Sci. 7, 63–78.

İnci, U., 2002. Depositional evolution of Miocene coal successions in the Soma coalfield, western Turkey. Int. J. Coal Geol. 51, 1–29.

International Committee for Coal Petrology (ICCP), 1994. The new vitrinite classification (ICCP System 1994). Fuel 77, 349–358.

International Committee for Coal Petrology (ICCP), 2001. The new inertinite classification (ICCP System 1994). Fuel 80, 459–471.

International Organization for Standardization (ISO) 7404–5, 2009. Methods for the Petrographic Analysis of Coal —Part 5: Method of Determining microscopically the Reflectance of Vitrinite. International Organization for Standardization, Geneva, Switzerland (14 pp).

International Standard Organisation (ISO) 11760, 2005. Classification of Coals. International Organization for Standardization, Geneva, Switzerland (99 pp).

International Standard Organization (ISO) 7404–2, 2009. Methods for the Petrographic Analysis of Coals — Part 2: Methods of Preparing Coal Samples. International Organization for Standardization, Geneva, Switzerland (12 pp).

Kalaitzidis, S., Bouzinos, A., Papazisimou, S., Christanis, K., 2004. A short-term establishment of forest fen habitat during Pliocene lignite formation in the Ptolemais Basin, NW Macedonia, Greece. Int. J. Coal Geol. 57, 243–263.

Kalaitzidis, S., Siavalas, G., Skarpelis, N., Araujo, C.V., Christanis, K., 2009. Late Cretaceous coal overlying karstic bauxite deposits in the Parnassus-Ghiona Unit, Central Greece: coal characteristics and depositional environment. Int. J. Coal Geol. 81, 211–226.

Kalkreuth, W.D., Marchioni, D.L., Calder, J.H., Lamberson, M.N., Naylor, R.D., Paul, J., 1991. The relationship between coal petrography and depositional environments from selected coal basins in Canada. Int. J. Coal Geol. 19, 21–76.

Karayiğit, A.İ., 1998. Thermal effects of a basaltic intrusion on the Soma lignite bed in west Turkey. Energy Sources 20, 55–66.

Karayiğit, A.İ., Whateley, M.K.G., 1997. Properties of a lacustrine subbituminous (kl) seam, with special reference to the contact metamorphism. Soma-Turkey. Int. J. Coal Geol. 34, 131–155.

Karayiğit, A.I., Gayer, R.A., Querol, X., Onacak, T., 2000. Contents of major and trace elements in feed coals from Turkish coal-fired power plants. Int. J. Coal Geol. 44, 169–184.

Karayiğit, A.I., Gayer, R.A., Ortac, F.E., Goldsmith, S., 2001. Trace elements in the Lower Pliocene fossiliferous Kangal lignites, Sivas, Turkey. Int. J. Coal Geol. 47, 73–89.

Karayiğit, A.I., Bulut, Y., Querol, X., Alastuey, A., Vassilev, S., 2006. Variations in fly ash composition from the Soma power plant, Turkey. Energy Sources 27, 1473–1481.

Karayiğit, A.I., Oskay, R.G., Christanis, K., Tunoğlu, C., Tuncer, A., Bulut, Y., 2015. Palaeoenvironmental reconstruction of the Çardak coal seam, SW Turkey. Int. J. Coal Geol. 139, 3–16.

Karayiğit, A.I., Oskay, R.G., Tuncer, A., Mastalerz, M., Gümüş, B.A., Şengüler, I., Yaradılmış, H., Tunoğu, C., 2016. A multidisciplinary study of the Gölbaşı–Harmanlı coal seam, SE Turkey. Int. J. Coal Geol. 167, 31–47.
Karayiğit, A.I., Bircan, C., Mastalerz, M., Oskay, R.G., Querol, X., Lieberman, N.R., Türkmen, İ., 2017. Coal characteristics, elemental composition and modes of occurrence of some elements in the İsaalan coal (Balıkesir, NW Turkey). Int. J. Coal Geol. 172, 43–59.
Kayseri-Özer, S., 2017. Cenozoic vegetation and climate change in Anatolia - a study based on the IPR-vegetation analysis. Palaeogeogr. Palaeoclimatol. Palaeoecol. 467, 37–68.
Ketris, M.P., Yudovich, Ya.E., 2009. Estimations of Clarkes for carbonaceous biolithes: world averages for trace element contents in black shales and coals. Int. J. Coal Geol. 78, 135–148.
Killops, S.D., Funnell, R.H., Suggate, R.P., Sykes, R., Peters, K.E., Walters, C., Woolhouse, A.D., Weston, R.J., Boudou, J.-P., 1998. Predicting generation and expulsion of paraffinic oil from vitrinite-rich coals. Org. Geochem. 29, 1–21.
Kolcon, I., Sachsenhofer, R.F., 1999. Petrography, palynology and depositional environments of the early Miocene Oberdorf lignite seam (Styrian Basin, Austria). Int. J. Coal Geol. 41, 275–308.
Koukouzas, N., Ward, C.R., Li, Z., 2010a. Mineralogy of lignites and associated strata in the Mavropigi field of the Ptolemais Basin, northern Greece. Int. J. Coal Geol. 81, 182–190.
Koukouzas, N., Kalaitzidis, S.P., Ward, C.R., 2010b. Organic petrographical, mineralogical and geochemical features of the Achlada and Mavropigi lignite deposits, NW Macedonia, Greece. Int. J. Coal Geol. 83, 387–395.
Kramer, W., Weatherall, G., Offler, R., 2001. Origin and correlation of tuffs in the Permian Newcastle and Wollombi Coal Measures, NSW, Australia, using chemical fingerprinting. Int. J. Coal Geol. 47, 115–135.
Li, Z., Ward, C.R., Gurba, L.W., 2007. Occurrence of non-mineral inorganic elements in low-rank coal macerals as shown by electron microprobe element mapping techniques. Int. J. Coal Geol. 70, 137–149.
Li, Z., Ward, C.R., Gurba, L.W., 2010. Occurrence of non-mineral inorganic elements in macerals of low-rank coals. Int. J. Coal Geol. 81, 242–250.
Li, B., Zhuang, X., Li, J., Querol, X., Font, O., Moreno, N., 2017. Enrichment and distribution of elements in the Late Permian coals from the Zhina Coalfield, Guizhou Province, Southwest China. Int. J. Coal Geol. 171, 111–129.
Mitrović, D., Đoković, N., Životić, D., Bechtel, A., Šajnović, A., Stojanović, K., 2016. Petrographical and organic geochemical study of the Kovin lignite deposit, Serbia. Int. J. Coal Geol. 168, 80–107.
Mukhopadhyay, P., 1989. Organic petrography and organic geochemistry of tertiary coals from texas in relation to depositional environment and hydrocarbon generation. Report of Investigations. Bureau of Economic Geology, Texas (118 pp).
Nebert, K., 1978. Das braunkohlenführende Neogengebiet von Soma, Westanatolien. Bull. Min. Res. Expl. 90, 20–72.
Oikonomopoulos, I., Kaouras, G., Antoniadis, P., Perraki, T., Gregor, H.-J., 2008. Neogene Achlada lignite deposits in NW Greece. Bull. Geosci. 83, 335–349.
Oikonomopoulos, I.K., Kaouras, G., Tougiannidis, N., Ricken, W., Gurk, M., Antoniadis, P., 2015. The depositional conditions and the palaeoenvironment of the Achlada xylite-dominated lignite in western Makedonia, Greece. Palaeogeogr. Palaeoclimatol. Palaeoecol. 440, 777–792.
O'Keefe, J.M.K., Bechtel, A., Christanis, K., Dai, S., Di Michele, W.A., Eble, C.F., Esterle, J.S., Mastalerz, M., Raymond, A.L., Valentim, B.V., Wagner, N.J., Ward, C.R., Hower, J.C., 2013. On the fundamental difference between coal rank and coal type. Int. J. Coal Geol. 118, 58–87.
Oskay, R.G., Christanis, K., İnaner, H., Salman, M., Taka, M., 2016. Palaeoenvironmental reconstruction of the eastern part of the Karapınar-Ayrancı coal deposit (Central Turkey). Int. J. Coal Geol. 163, 100–111.
Pepper, A.S., Corvi, P.J., 1995. Simple kinetic models of petroleum formation. Part I: oil and gas generation from kerogen. Mar. Pet. Geol. 12, 291–319.
Permana, A.K., Ward, C.R., Li, Z., Gurba, L.W., 2013. Distribution and origin of minerals in high-rank coals of the South Walker Creek area, Bowen Basin, Australia. Int. J. Coal Geol. 116–117, 185–207.
Peters, K.E., 1986. Guidelines for evaluating petroleum source rock using programmed pyrolysis. AAPG Bull. 70, 318–329.
Peters, K.E., Moldowan, J.M., 1993. The Biomarker Guide: Interpreting Molecular Fossils in Petroleum and Ancient Sediments. Prentice Hall, Englewood Cliff (363 pp).
Petersen, H.I., 2006. The petroleum generation potential and effective oil window of humic coals related to coal composition and age. Int. J. Coal Geol. 67, 221–248.
Petersen, H.I., Rosenberg, P., 2000. The relationship between the composition and rank of humic coals and their activation energy distributions for the generation of bulk petroleum. Pet. Geosci. 6, 137–149.
Petersen, H.I., Lindström, S., Nytoft, H.P., Rosenberg, P., 2009. Composition, peat-forming vegetation and kerogen paraffinicity of Cenozoic coals: relationship to variations in the petroleum generation potential (Hydrogen Index). Int. J. Coal Geol. 78, 119–134.
Pickel, W., Kus, J., Flores, D., Kalaitzidis, S., Christanis, K., Cardott, B.J., Misz-Kennan, M., Rodrigues, S., Hentschel, A., Hamor-Vido, M., Crosdale, P., Wagner, N., ICCP, 2017. Classification of liptinite – ICCP System 1994. Int. J. Coal Geol. 169, 40–61.
Poppe, L.J., Paskevich, V.F., Hathaway, J.C., Blackwood, D.S., 2001. A laboratory manual for x-ray powder diffraction. U. S. Geological Survey Open-File Report 01-041 Avaiable at. https://pubs.usgs.gov/of/2001/of01-041/index.htm (Accessed 20 May 2016).
Querol, X., Fernández-Turiel, J., López-Soler, A., 1995. Trace elements in coal and their behaviour during combustion in a large power station. Fuel 74, 331–343.
Querol, X., Cabrera, L.I., Pickel, W., López-Soler, A., Hagemann, H.W., Fernández-Turiel, J.L., 1996. Geological controls on the coal quality of the Mequinenza subbituminous coal deposit, northeast Spain. Int. J. Coal Geol. 29, 67–91.
Querol, X., Whateley, M.K.G., Fernández-Turiel, J.L., Tuncalı, E., 1997. Geological controls on the mineralogy and geochemistry of the Beypazari lignite, central Anatolia, Turkey. Int. J. Coal Geol. 33, 255–271.
Querol, X., Alastuey, A., Plana, F., Lopez-Soler, A., Tuncali, E., Toprak, S., Ocakoglu, F., Koker, A., 1999. Coal geology and coal quality of the Miocene Mugla basin, southwestern Anatolia, Turkey. Int. J. Coal Geol. 41, 311–332.
Ruppert, L.F., Moore, T.A., 1993. Differentiation of volcanic ash-fall and water-borne detrital layers in the Eocene Senakin coal bed, Tanjung Formation, Indonesia. Org. Geochem. 20, 233–247.
Seyitoğlu, G., Scott, B., 1991. Late Cenozoic crustal extension and basin formation in west Turkey. Geol. Mag. 128, 155–166.
Seyitoğlu, G., Scott, B., 1996. The cause of N–E extensional tectonics in western Turkey: tectonic escape vs. back-arc spreading vs. orogenic collapse. J. Geodyn. 22, 145–153.
Shoval, S., Panczer, G., Boudeulle, M., 2008. Study of the occurrence of titanium in kaolinites by micro-Raman spectroscopy. Opt. Mater. 30, 1699–1705.
Siavalas, G., Linou, M., Chatziapostolou, A., Kalaitzidis, S., Papaefthymiou, H., Christanis, K., 2009. Palaeoenvironment of Seam I in the Marathousa Lignite Mine, Megalopolis Basin (Southern Greece). Int. J. Coal Geol. 78, 233–248.
Spears, D.A., 2012. The origin of tonsteins, an overview, and links with seatearths, fireclays and fragmental clay rocks. Int. J. Coal Geol. 94, 22–31.
Swaine, D.J., 1990. Trace Elements in Coal. Butterworths, London (278 pp).
Sykes, R., Snowdon, L.R., 2002. Guidelines for assessing the petroleum potential of coaly source rocks using Rock-Eval pyrolysis. Org. Geochem. 33, 1441–1455.
Sýkorová, I., Pickel, W., Christanis, K., Wolf, M., Taylor, G.H., Flores, D., 2005. Classification of huminite — ICCP System 1994. Int. J. Coal Geol. 62, 85–106.
Takahashi, K., Jux, U., 1991. Miocene palynomorphs from lignites of the Soma Basin (west Anatolia, Turkey). Bull. Fac. Liberal Arts, Nagasaki Unv. Nat. Sci. 32, 7–165.
Tercan, A.E., Ünver, B., Hindistan, M.A., Ertunç, G., Atalay, F., Ünal, S., Killioğlu, Y., 2013. Seam modelling and resource estimation in the coalfields of western Anatolia. Int. J. Coal Geol. 112, 94–106.
Tissot, B.P., Welte, D.H., 1984. Petroleum and Formation Occurrence. Springer, Berlin (699 pp).
Toprak, S., 2009. Petrographic properties of major coal seams in Turkey and their formation. Int. J. Coal Geol. 78, 263–275.
Triplehorn, D.M., Stanton, R.W., Ruppert, L.F., Crowley, S.S., 1991. Volcanic ash dispersed in the Wyodak-Anderson coal bed, Powder River Basin, Wyoming. Org. Geochem. 17, 567–575.
Tuncalı, E., Çiftci, B., Yavuz, N., Toprak, S., Köker, A., Gencer, Z., Ayçık, H., Pahin, N., 2002. Chemical and Technological Properties of Turkish Tertiary Coals. MTA Publication, Ankara (401 pp).
Turkish Lignite Company-Aegean Lignite Cooperation (TKİ-ELİ), 2015. The Annual Report of 2015. (Soma-Manisa, Turkey, 23 pp). Accessible at http://www.eli.gov.tr, accessed 28 October 2016.
Vassilev, S.V., Vassileva, C.G., Karayiğit, A.I., Bulut, Y., Alastuey, A., Querol, X., 2005. Phase-mineral and chemical composition of composite samples from feed coals, bottom ashes and fly ashes at the Soma power station, Turkey. Int. J. Coal Geol. 61, 35–63.
Volkman, J.K., 1986. A review of sterol markers for marine and terrigenous organic matter. Org. Geochem. 9, 83–99.
Ward, C.R., 1991. Mineral matter in low-rank coals and associated strata of the Mae Moh basin, northern Thailand. Int. J. Coal Geol. 17, 69–93.
Ward, C.R., 2016. Analysis, origin and significance of mineral matter in coal: an updated review. Int. J. Coal Geol. 165, 1–27.
Ward, C.R., Spears, D.A., Booth, C.A., Staton, I., Gurba, L.W., 1999. Mineral matter and trace elements in coals of the Gunnedah Basin, New South Wales, Australia. Int. J. Coal Geol. 40, 281–308.
Weiss, H.M., Wilhelms, A., Mills, N., Scotchmer, J., Hall, P.B., Lind, K., Brekke, T., 2000. NIGOGA - The Norwegian Industry Guide to Organic Geochemical Analyses. fourth ed. Published by Norsk Hydro, Statoil, Geolab Nor, SINTEF Petroleum Research and the Norwegian Petroleum Directorate, Oslo (102 pp).
Wilkins, R.W.T., George, S.C., 2002. Coal as a source rock for oil: a review. Int. J. Coal Geol. 50, 317–361.
Yılmaz, Y., Genç, Ş.C., Gürer, F., Bozcu, M., Yılmaz, K., Karacık, Z., Altunkaynak, S., Elmas, A., Bozkurt, E., Winchester, J.A., Piper, J.A.D., 2000. When did the western Anatolian grabens begin to develop? Tectonics and Magmatism in Turkey and the Surrounding Area. 173. Geol. Soc. London, pp. 131–162 (Spec. Publ.)
Zhao, L., Ward, C.R., French, D., Graham, I.T., 2012. Mineralogy of the volcanic-influenced Great Northern coal seam in the Sydney Basin, Australia. Int. J. Coal Geol. 94, 94–110.
Zhao, L., Dai, S., Graham, I.T., Li, X., Zhang, B., 2016a. New insights into the lowest Xuanwei Formation in easternYunnan Province, SW China: implications for Emeishan large igneous province felsic tuff deposition and the cause of the end-Guadalupian mass extinction. Lithos 264, 375–391.
Zhao, L., Sun, J., Guo, W., Wang, P., Ji, D., 2016b. Mineralogy of the Pennsylvanian coal seam in the Datanhao mine, Daqingshan Coalfield, Inner Mongolia, China: genetic implications for mineral matter in coal deposited in an intermontane basin. Int. J. Coal Geol. 167, 201–214.
Zhao, L., Dai, S., Graham, I.T., Li, X., Liu, H., Song, X., Hower, J.C., Zhou, Y., 2017. Cryptic sediment-hosted critical element mineralization from eastern Yunnan Province, southwestern China: mineralogy, geochemistry, relationship to Emeishan alkaline magmatism and possible origin. Ore Geol. Rev. 80, 116–140.
Zhou, Y., Ren, Y., Tang, D., Bohor, B., 1994. Characteristics of zircons from volcanic ash-derived tonsteins in Late Permian coal fields of eastern Yunnan, China. Int. J. Coal Geol. 25, 243–264.
Zhou, Y., Bohor, B.F., Ren, Y., 2000. Trace element geochemistry of altered volcanic ash layers (tonsteins) in late Permian coal-bearing formations of eastern Yunnan and western Guizhou Provinces, China. Int. J. Coal Geol. 44, 305–324.